

Electroweak symmetry breaking after the Higgs discovery

S. Dawson

Brookhaven National Laboratory, Upton, New York, USA

Abstract

I give a pedagogical introduction to the physics of electroweak symmetry breaking. Higgs boson production and decay at the LHC and the consistency of the Higgs measurements with triviality arguments, vacuum stability, and precision electroweak measurements are discussed. Effective Lagrangian techniques are used to understand potential deviations from the Standard Model (SM) predictions.

Keywords

Lectures; Higgs boson; Oblique parameters; Triviality; Effective Field Theory

1 Introduction

The experimental discovery of the Higgs boson [1, 2] implies that the Weinberg Salam Standard Model (SM) is a valid low energy theory at the weak scale. All current measurements are consistent with this statement and physics in the electroweak symmetry breaking (EWSB) sector beyond that predicted by the SM is highly constrained by current experimental results, both at the LHC and from precision electroweak measurements. These lectures summarize the underlying theoretical framework of the SM and its experimental predictions and discuss possible high scale extensions of the theory in terms of an effective field theory.

Section 2 contains an introduction to the SM and Section 3 discusses theoretical restrictions on the EWSB sector. Section 4 presents the basics of Higgs production and decay, along with a summary of experimental results. Pedagogical discussions of the gluon fusion production rate at leading order and the determination of the Higgs width are also found in Section 4. Extensions of the SM in terms of an effective field theory are presented in Section 5 and Section 6 contains some conclusions. There are many excellent reviews of Higgs physics and the reader is referred to them for additional details and further references [3–9].

2 Weinberg-Salam Model

The Weinberg-Salam model is an $SU(2)_L \times U(1)_Y$ gauge theory containing three $SU(2)_L$ gauge bosons, W_μ^I , $I = 1, 2, 3$, and one $U(1)_Y$ gauge boson, B_μ , with kinetic energy terms,

$$\mathcal{L}_{\text{KE}} = -\frac{1}{4}W_{\mu\nu}^I W^{\mu\nu I} - \frac{1}{4}B_{\mu\nu}B^{\mu\nu}, \quad (1)$$

where the index I is summed over and,

$$\begin{aligned} W_{\mu\nu}^I &= \partial_\nu W_\mu^I - \partial_\mu W_\nu^I + g\epsilon^{IJK}W_\mu^J W_\nu^K, \\ B_{\mu\nu} &= \partial_\nu B_\mu - \partial_\mu B_\nu. \end{aligned} \quad (2)$$

The $SU(2)_L$ and $U(1)_Y$ coupling constants are g and g' , respectively. Coupled to the gauge fields is a complex scalar $SU(2)$ doublet, Φ ,

$$\Phi = \begin{pmatrix} \phi^+ \\ \phi^0 \end{pmatrix}. \quad (3)$$

The scalar potential is given by,

$$V(\Phi) = \mu^2 |\Phi^\dagger \Phi| + \lambda \left(|\Phi^\dagger \Phi| \right)^2, \quad (4)$$

where $\lambda > 0$.

The state of minimum energy for $\mu^2 < 0$ is not at $\phi^0 = 0$ and the scalar field develops a VEV¹. The direction of the minimum in $SU(2)_L$ space is not determined, since the potential depends only on the combination $\Phi^\dagger \Phi$ and we arbitrarily choose

$$\langle \Phi \rangle \equiv \frac{1}{\sqrt{2}} \begin{pmatrix} 0 \\ v \end{pmatrix}. \quad (5)$$

With this choice, the electromagnetic charge is,²

$$Q = \frac{(\tau_3 + Y)}{2}, \quad (6)$$

where we assign hypercharge $Y = 1$ to Φ .

Therefore,

$$Q\langle \Phi \rangle = 0 \quad (7)$$

and electromagnetism is unbroken by the scalar VEV. The VEV of Equation (5) yields the desired symmetry breaking pattern,

$$SU(2)_L \times U(1)_Y \rightarrow U(1)_{EM}. \quad (8)$$

The scalar contribution to the Lagrangian is,

$$\mathcal{L}_s = (D^\mu \Phi)^\dagger (D_\mu \Phi) - V(\Phi), \quad (9)$$

where³

$$D_\mu = \partial_\mu + i\frac{g}{2}\tau \cdot W_\mu + i\frac{g'}{2}B_\mu Y. \quad (10)$$

In unitary gauge there are no Goldstone bosons and only the physical Higgs scalar remains in the spectrum after spontaneous symmetry breaking. In unitary gauge,

$$\Phi = \frac{1}{\sqrt{2}} \begin{pmatrix} 0 \\ v + h \end{pmatrix}, \quad (11)$$

which gives the contribution to the gauge boson masses from the scalar kinetic energy term of Equation (9),

$$M^2 \sim \frac{1}{2}(0, v) \left(\frac{1}{2}g\tau \cdot W_\mu + \frac{1}{2}g'B_\mu \right)^2 \begin{pmatrix} 0 \\ v \end{pmatrix}. \quad (12)$$

The physical gauge fields are two charged fields, W^\pm , and two neutral gauge bosons, Z and γ .

$$\begin{aligned} W_\mu^\pm &= \frac{1}{\sqrt{2}}(W_\mu^1 \mp iW_\mu^2) \\ Z^\mu &= \frac{-g'B_\mu + gW_\mu^3}{\sqrt{g^2 + g'^2}} \equiv -\sin\theta_W B_\mu + \cos\theta_W W_\mu^3 \end{aligned}$$

¹There is no mechanism or motivation for determining the sign(μ^2) in the SM.

²The τ_I are the Pauli matrices with $Tr(\tau_I \tau_J) = 2\delta_{IJ}$.

³Different choices for the gauge kinetic energy and the covariant derivative depend on whether g and g' are chosen positive or negative. There are no physical consequences of this choice.

$$A^\mu = \frac{gB_\mu + g'W_\mu^3}{\sqrt{g^2 + g'^2}} \equiv \cos \theta_W B_\mu + \sin \theta_W W_\mu^3. \quad (13)$$

Equation (13) defines a mixing angle,

$$\sin \theta_W \equiv \frac{g'}{\sqrt{g^2 + g'^2}}. \quad (14)$$

Since the massless photon must couple with electromagnetic strength, e , the coupling constants define the weak mixing angle θ_W ,

$$\begin{aligned} e &= g \sin \theta_W \equiv g s_W \\ e &= g' \cos \theta_W \equiv g' c_W. \end{aligned} \quad (15)$$

The gauge bosons obtain masses from the Higgs mechanism, as demonstrated in Equation (12):

$$M_W^2 = \frac{1}{4}g^2v^2, \quad M_Z^2 = \frac{1}{4}(g^2 + g'^2)v^2, \quad M_A = 0. \quad (16)$$

If we go to a gauge other than unitary gauge, there are Goldstone bosons in the spectrum and the scalar field can be parameterized,

$$\Phi = \frac{1}{\sqrt{2}}e^{i\frac{\omega \cdot \tau}{2v}} \begin{pmatrix} 0 \\ v + h \end{pmatrix}. \quad (17)$$

In the Standard Model, there are three Goldstone bosons, $\vec{\omega} = (\omega^\pm, z)$, with masses M_W and M_Z in the Feynman gauge.

Fermions can easily be included in the theory. We write the fermions in terms of their left- and right-handed projections,

$$\psi_{L,R} = \frac{1}{2}(1 \mp \gamma_5)\psi. \quad (18)$$

From the four-Fermi theory of weak interactions [9], we know experimentally that the W -boson couples only to left-handed fermions and so we construct the $SU(2)_L$ doublet,

$$L_L = \begin{pmatrix} \nu_L \\ e_L \end{pmatrix}. \quad (19)$$

From Equation (6), the hypercharge of the lepton doublet must be $Y_L = -1$. In the limit where the neutrino is massless, it can have only one helicity state which is taken to be ν_L . Including neutrino masses requires interactions beyond the standard construction of the Weinberg-Salam model⁴. The SM is therefore constructed with no right-handed neutrinos. Further, we assume that right-handed fields do not interact with the W boson, and so the right-handed electron, e_R , must be an $SU(2)_L$ singlet with $Y_{e_R} = -2$. Using these hypercharge assignments, the leptons can be coupled in a gauge invariant manner to the $SU(2)_L \times U(1)_Y$ gauge fields,

$$\mathcal{L}_{lepton} = i\bar{e}_R\gamma^\mu \left(\partial_\mu + i\frac{g'}{2}Y_e B_\mu \right) e_R + i\bar{L}_L\gamma^\mu \left(\partial_\mu + i\frac{g}{2}\tau \cdot W_\mu + i\frac{g'}{2}Y_L B_\mu \right) L_L. \quad (20)$$

All of the known fermions can be accommodated in the Standard Model in this fashion. The $SU(2)_L$ and $U(1)_Y$ charge assignments of the first generation of fermions are given in Table 1. The quantum numbers of the 2nd and 3rd generation are identical to those of first generation.

⁴A pedagogical introduction to ν masses can be found in Ref. [10].

Field	SU(3)	$SU(2)_L$	$U(1)_Y$
$Q_L = \begin{pmatrix} u_L \\ d_L \end{pmatrix}$	3	2	$\frac{1}{3}$
u_R	3	1	$\frac{4}{3}$
d_R	3	1	$-\frac{2}{3}$
$L_L = \begin{pmatrix} \nu_L \\ e_L \end{pmatrix}$	1	2	-1
e_R	1	1	-2
$\Phi = \begin{pmatrix} \phi^+ \\ \phi^0 \end{pmatrix}$	1	2	1

Table 1: Quantum numbers of the SM fermions.

A fermion mass term takes the form

$$\mathcal{L}_{mass} = -m\bar{\psi}\psi = -m\left(\bar{\psi}_L\psi_R + \bar{\psi}_R\psi_L\right). \quad (21)$$

As is obvious from Table 1, the left- and right-handed fermions transform differently under $SU(2)_L$ and $U(1)_Y$ gauge transformations and so gauge invariance forbids a term like Equation (21). The Higgs boson, however, can couple in a gauge invariant fashion to the down quarks,

$$\mathcal{L}_d = -Y_d\bar{Q}_L\Phi d_R + h.c., \quad (22)$$

After the Higgs obtains a VEV, we have the effective coupling,

$$-Y_d\frac{1}{\sqrt{2}}(\bar{u}_L, \bar{d}_L) \begin{pmatrix} 0 \\ v+h \end{pmatrix} d_R + h.c. \quad (23)$$

which can be seen to yield a mass term for the down quark,

$$Y_d = \frac{m_d\sqrt{2}}{v}. \quad (24)$$

In order to generate a mass term for the up-type quarks we use the fact that

$$\tilde{\Phi} \equiv i\tau_2\Phi^* = \begin{pmatrix} \phi^0 \\ -\phi^- \end{pmatrix} \quad (25)$$

is an $SU(2)_L$ doublet, and write the $SU(2)_L$ invariant coupling

$$\mathcal{L}_u = -Y_u\bar{Q}_L\tilde{\Phi}u_R + h.c. \quad (26)$$

which generates a mass term for the up quark. Similar couplings can be used to generate mass terms for the charged leptons. Since the neutrino has no right handed partner in the SM, it remains massless.

For the multi-family case, the Yukawa couplings, Y_d and Y_u , become $N_F \times N_F$ matrices (where N_F is the number of families). Since the fermion mass matrices and Yukawa matrices are proportional, the interactions of the Higgs boson with the fermion mass eigenstates are flavor diagonal and the Higgs boson does not mediate flavor changing interactions. This is an important prediction of the SM.

The parameter v can be found from the charged current for μ decay, $\mu \rightarrow e\bar{\nu}_e\nu_\mu$, which is measured very accurately to be $G_F = 1.16638 \times 10^{-5} \text{ GeV}^{-2}$. Since the momentum carried by the W boson is of order m_μ it can be neglected in comparison with M_W and we make the identification,

$$\frac{G_F}{\sqrt{2}} = \frac{g^2}{8M_W^2} = \frac{1}{2v^2}, \quad (27)$$

which gives the result

$$v = (\sqrt{2}G_F)^{-1/2} = 246 \text{ GeV} . \quad (28)$$

One of the most important points about the Higgs mechanism is that all of the couplings of the Higgs boson to fermions and gauge bosons are completely determined in terms of coupling constants and fermion masses. A complete set of Feynman rules can be found in Ref. [5]. The potential of Equation (4) had two free parameters, μ and λ , which can be traded for,

$$\begin{aligned} v^2 &= -\frac{\mu^2}{2\lambda} \\ m_h^2 &= 2v^2\lambda . \end{aligned} \quad (29)$$

The scalar potential is now,

$$V = \frac{m_h^2}{2}h^2 + \frac{m_h^2}{2v}h^3 + \frac{m_h^2}{8v^2} . \quad (30)$$

The self-interactions of the Higgs boson are determined in terms of the Higgs mass. There are no remaining adjustable parameters and so Higgs production and decay processes can be computed unambiguously in terms of the Higgs mass.

3 Theoretical Constraints

3.1 Bounds from Precision Measurements

The Higgs boson enters into one loop radiative corrections in the Standard Model and precision electroweak measurements test the consistency of the theory⁵. In the electroweak sector of the SM, there are four fundamental parameters, the $SU(2)_L \times U(1)_Y$ gauge coupling constants, g and g' , as well as the two parameters of the Higgs potential, which are usually taken to be the vacuum expectation value of the Higgs boson, v , and the Higgs mass, m_h . Once these parameters are fixed, all other physical quantities can be derived in terms of them (and of course the fermion masses and CKM mixing parameters, along with the strong coupling constant α_s). Equivalently, the muon decay constant, G_μ , the Z-boson mass, M_Z , and the fine structure constant, α , can be used as input parameters. Experimentally, the measured values for these input parameters are [11, 12],

$$\begin{aligned} G_\mu &= 1.16638(1) \times 10^{-5} \text{ GeV}^{-2} \\ M_Z &= 91.1876(21) \text{ GeV} \\ \alpha^{-1} &= 137.035999679(94) \\ m_h &= 125.09 \pm .21(stat) \pm .11(syst) \text{ GeV} . \end{aligned} \quad (31)$$

The W boson mass is thus a prediction of the theory and is defined through muon decay,

$$\begin{aligned} M_W^2 &= \frac{\pi\alpha}{\sqrt{2}G_\mu(1 - M_W^2/M_Z^2)} \\ M_W^2 &= \frac{M_Z^2}{2} \left\{ 1 + \sqrt{1 - \frac{4\pi\alpha}{\sqrt{2}G_\mu M_Z^2}} \right\} . \end{aligned} \quad (32)$$

⁵An introductory review of precision measurements in the SM can be found in Ref. [13].

At tree level, the SM prediction from Equation (32) is,

$$M_W(\text{tree}) = 79.829 \text{ GeV}, \quad (33)$$

in slight disagreement with the measured value [11],

$$M_W(\text{experiment}) = 80.379 \pm 0.012 \text{ GeV}. \quad (34)$$

In order to obtain good agreement between theory and the experimental data, it is crucial to include radiative corrections. The prediction for M_W can be written as [14],

$$M_W^2 = \frac{\pi\alpha}{\sqrt{2}G_\mu s_W^2} \left[1 + \Delta r_{SM} \right], \quad (35)$$

where Δr_{SM} summarizes the radiative corrections. The dependence on the top quark mass, m_t , is particularly significant as Δr_{SM} depends on m_t quadratically,

$$\Delta r_{SM}^t = -\frac{G_\mu N_c}{\sqrt{2} 8\pi^2} \left(\frac{c_W^2}{s_W^2} \right) m_t^2 + \log(m_t) \text{ terms}, \quad (36)$$

where $N_c = 3$ is the number of colors. The dependence on m_h is logarithmic,

$$\Delta r_{SM}^h \sim \frac{\alpha}{\pi s_W^2} \frac{11}{48} \log\left(\frac{m_h^2}{M_Z^2}\right) + \mathcal{O}\left(\frac{m_h^2}{M_Z^2}, \frac{v^4}{\Lambda^4}\right). \quad (37)$$

The top quark does not decouple from the theory even at energies far above the top quark mass. This is because the top quark coupling to the Higgs boson is proportional to m_t .

The agreement between the radiatively corrected prediction for the W mass given by Equation (35) with the measured value is a strong test of the theory. In a similar fashion, the full set of electroweak data can be used to test the self consistency of the theory, as demonstrated in Figure 1 [15]. Similar studies have been performed by the GFITTER collaboration [16]. (The most restrictive data points are the measurements of the $Zb\bar{b}$ coupling and the W boson mass.) When the experimental values of M_W , m_t , and m_h are omitted, the fit is in good agreement with the directly measured values of the masses. Note that the fit excludes a large ($\sim 100's$ of GeV) value of m_h and so even before the Higgs boson was discovered, we knew that if there were no new physics contributions to the predictions for electroweak quantities such as M_W , the Higgs boson could not be too heavy.

3.2 Oblique Parameters

Extensions of the SM with modified Higgs sectors are significantly restricted by the requirement of consistency with the electroweak measurements. A simple way to examine whether a theory with a complicated Higgs sector is consistent with electroweak experiments is to use the oblique parameters. Using the oblique parameters to obtain limits on BSM physics assumes that the dominant contributions resulting from the expanded theory are to the gauge boson 2-point functions [17, 18]. Combinations of the 2- point functions define S, T and U . New physics effects are determined by subtracting the SM contribution, e.g. $\Delta S \equiv S_{BSM} - S_{SM}$.

A simple example is a model with a real scalar singlet, S , added to the SM. After imposing a Z_2 symmetry under which $S \rightarrow -S$, the most general scalar potential is [19]

$$V = -\mu^2 \Phi^\dagger \Phi - m^2 S^2 + \lambda(\Phi^\dagger \Phi)^2 + \frac{a_2}{2} \Phi^\dagger \Phi S^2 + \frac{b_4}{4} S^4. \quad (38)$$

After spontaneous symmetry breaking, both Φ and S obtain VEVs and the mass eigenstates h and H are a mixture of S and Φ ($s \equiv \langle S \rangle$),

$$\begin{pmatrix} h \\ H \end{pmatrix} = \begin{pmatrix} \cos \alpha & -\sin \alpha \\ \sin \alpha & \cos \alpha \end{pmatrix} \begin{pmatrix} \sqrt{2}\phi_0 - v \\ S - s \end{pmatrix}, \quad (39)$$

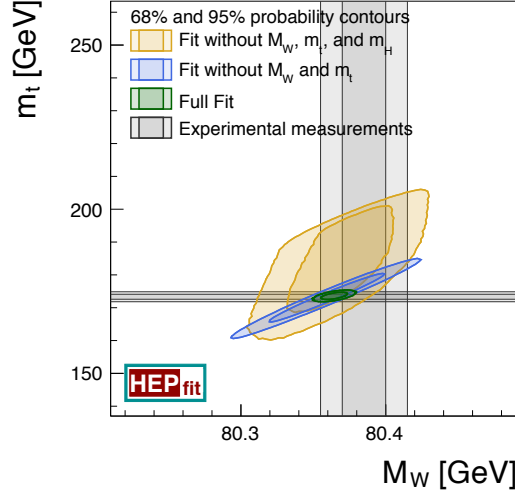


Fig. 1: Experimental limits on M_W and m_t from precision electroweak measurements. The straight bands are the direct measurements of M_W and m_t [15].

with physical masses, m_h and M_H . The singlet cannot couple directly to fermions or gauge bosons, so the only physical effect on single Higgs production is through the mixing of Equation (39). The mixing affects the SM-like Higgs couplings to both fermions and gauge bosons in an identical fashion and all SM couplings are suppressed by the factor $\cos \alpha$. This model is particularly simple since it can be studied in terms of M_H and the mixing angle α . For $m_h, M_H \gg M_W, M_Z$, the contributions to the oblique parameters are,

$$\begin{aligned}
 \Delta S &= \frac{1}{12\pi} \sin^2 \alpha \log \left(\frac{M_H^2}{m_h^2} \right) \\
 \Delta T &= -\frac{3}{16\pi c_W^2} \sin^2 \alpha \log \left(\frac{M_H^2}{m_h^2} \right) \\
 \Delta U &= 0.
 \end{aligned} \tag{40}$$

and for any given value of M_H , an upper limit on $\sin \alpha$ can be determined [20]. Limits from the oblique parameters are an important tool in understanding what BSM models are allowed experimentally and in restricting the parameters of the models.

3.3 Restrictions from Triviality

Theoretical bounds on the Higgs boson mass can be deduced on the grounds of *triviality*, which can be summarized as the requirement that the Higgs quartic coupling remain finite at high energy scales. If the quartic coupling becomes infinite, the theory is no longer perturbative, while if the quartic coupling goes to zero, the theory is non-interacting. The Higgs quartic coupling, λ , changes with the effective energy scale, Λ , due to the self interactions of the scalar field:

$$\frac{d\lambda}{dt} = \frac{3\lambda^2}{4\pi^2}, \tag{41}$$

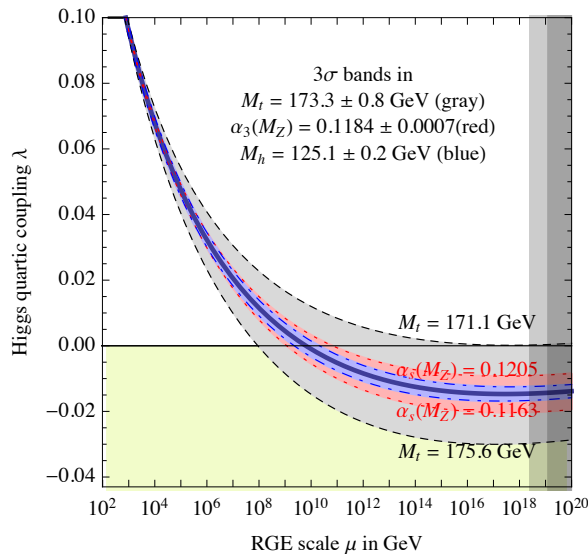


Fig. 2: Dependence of the Higgs quartic coupling on the renormalization scale [21].

where $t \equiv \log(\Lambda^2/v^2)$. In the SM, however, there are also contributions due to gauge boson and fermion loops⁶. Including the top quark contribution, Equation (42) becomes,

$$\frac{d\lambda}{dt} = \frac{3}{4\pi^2} \left\{ \lambda^2 - Y_t^2 \lambda - Y_t^4 \right\}, \quad (42)$$

where $Y_t = m_t/v$. For small λ (small m_h), the Y_t^4 term dominates and the quartic coupling decreases with energy,

$$\lambda(\Lambda) \sim \lambda(v) - \frac{3Y_t^4}{4\pi^2} \log\left(\frac{\Lambda^2}{v^2}\right). \quad (43)$$

The scaling of λ has been performed to 2– loops [21], including contributions from gauge and Yukawa couplings and the result is shown in Figure 2. The quartic coupling becomes negative at a high scale that is quite sensitive to m_t and α_s , suggesting that at this scale some new physics is required to force λ to be positive which is needed in order for the potential to be bounded from below.

4 Higgs Production and Decay

In this section we review the SM rates for Higgs production and decay. Numerical values, including the most precisely known higher order calculations, have been tabulated by the LHC Higgs cross section working group [22].

4.1 Higgs Decays

Expressions for the SM Higgs decay widths at leading order can be found in Ref. [5], and the QCD corrected rates, with references to the original literature, are given in Refs. [4, 8]. The QCD NLO corrected decay rates can be found using the public code, HDECAY [23].

⁶We neglect the gauge contributions here.

4.1.1 $h \rightarrow f\bar{f}$

The Higgs couplings to fermions are proportional to fermion mass and the lowest order width for the Higgs decay to fermions of mass m_f is,

$$\Gamma(h \rightarrow f\bar{f}) = \frac{G_F m_f^2 N_{ci}}{4\sqrt{2}\pi} m_h \beta_F^3, \quad (44)$$

where $\beta_F \equiv \sqrt{1 - 4m_f^2/m_h^2}$ is the velocity of the final state fermions and $N_{ci} = 1(3)$ for charged leptons (fermions). The largest fermion decay channel is $h \rightarrow b\bar{b}$, which receives large QCD corrections. A significant portion of the QCD corrections can be accounted for by expressing the decay width in terms of a running quark mass, $m_f(\mu)$, evaluated at the scale $\mu = m_h$. The QCD corrected decay width can then be approximated as [24, 25],

$$\Gamma(h \rightarrow q\bar{q}) = \frac{3G_F}{4\sqrt{2}\pi} m_q^2(m_h^2) m_h \beta_q^3 \left(1 + 5.67 \frac{\alpha_s(m_h^2)}{\pi} + \dots \right), \quad (45)$$

where $\alpha_s(m_h^2)$ is defined in the \overline{MS} scheme with 5 flavors. In leading log QCD, the running of the b quark mass is,

$$m_b(\mu^2) = m \left[\frac{\alpha_s(m^2)}{\alpha_s(\mu^2)} \right]^{(-12/23)} \left\{ 1 + \mathcal{O}(\alpha_s^2) \right\}, \quad (46)$$

where $m_b(m^2) \equiv m$ implies that the running mass at the position of the propagator pole is equal to the location of the pole. For $m_b(m_b^2) = 4.18 \text{ GeV}$, this yields an effective value $m_b(m_h = 125 \text{ GeV})|_{LL} = 2.8 \text{ GeV}$ (at NLL, $m_b(m_h = 125 \text{ GeV})|_{NLL} = 2.7 \text{ GeV}$). Inserting the QCD corrected mass into the expression for the width thus leads to a suppression of the width by $\sim .4$. Using the running b mass absorbs the large logarithms of the form $\log(m_h^2/m_b^2)$ and is important for numerical accuracy. The electroweak radiative corrections to $h \rightarrow f\bar{f}$ amount to only a few percent correction [26].

4.1.2 $h \rightarrow WW, ZZ$

The Higgs boson can also decay to gauge boson pairs. At tree level, the decays $h \rightarrow WW^*$ and $h \rightarrow ZZ^*$ are possible (with one of the gauge bosons off-shell), while at one-loop the decays $h \rightarrow gg, \gamma\gamma$, and γZ occur.

The decay width for the off-shell decay, $h \rightarrow ZZ^* \rightarrow f_1(p_1)f_2(p_2)Z(p_3)$, is,

$$\Gamma = \int_0^{(m_h - M_Z)^2} dq^2 \int dm_{23}^2 \frac{|A|^2}{256\pi^3 m_h^3}, \quad (47)$$

where $m_{ij} = (p_i + p_j)^2$, $m_{12}^2 \equiv q^2$, and $m_{12}^2 + m_{23}^2 + m_{13}^2 = m_h^2 + M_Z^2$, $\lambda(m_h^2, M_Z^2, q^2) \equiv q^4 - 2q^2(m_h^2 + M_Z^2) + (m_h^2 - M_Z^2)^2$, and $m_{23}^2|_{max,min} \equiv \frac{1}{2} \left(m_h^2 + M_Z^2 - q^2 \pm \sqrt{\lambda} \right)$. The amplitude-squared is,

$$|A(h \rightarrow Zf\bar{f})|^2 = 32 (g_L^2 + g_R^2) G_F^2 M_Z^4 \left[\frac{2M_Z^2 q^2 - m_{13}^2 q^2 - m_h^2 M_Z^2 + m_{13}^2 M_Z^2 + m_{13}^2 m_h^2 - m_{13}^4}{(q^2 - M_Z^2)^2 + \Gamma_Z^2 M_Z^2} \right], \quad (48)$$

with $g_{Lf} = T_{3f} - Q_f s_W^2$, $g_{Rf} = -Q_f s_W^2$, and $T_3 = \pm \frac{1}{2}$. We see that the amplitude is peaked at low q^2 . Integrating over dm_{23}^2 ,

$$\frac{d\Gamma}{dq^2}(h \rightarrow Zf\bar{f}) = (g_L^2 + g_R^2) G_F^2 \sqrt{\lambda(m_h^2, M_Z^2, q^2)} \frac{M_Z^4}{48\pi^3 m_h^3}$$

$$\cdot \left[\frac{(12M_Z^2 q^2 + \lambda(m_h^2, M_Z^2, q^2))}{(q^2 - M_Z^2)^2 + \Gamma_Z^2 M_Z^2} \right]. \quad (49)$$

The result for $h \rightarrow W f \bar{f}'$ can be found by making the appropriate redefinitions of the fermion - gauge boson couplings.

Performing the q^2 integral and summing over the final state fermions [27],

$$\begin{aligned} \Gamma(h \rightarrow WW^*) &= \frac{g^4 m_h}{512\pi^3} F\left(\frac{M_W}{m_h}\right) \\ \Gamma(h \rightarrow ZZ^*) &= \frac{g^4 m_h}{2048 \cos^4_W \pi^3} \left(7 - \frac{40}{3} s_W^2 + \frac{160}{9} s_W^4\right) F\left(\frac{M_Z}{m_h}\right), \end{aligned} \quad (50)$$

where

$$\begin{aligned} F(x) &= |1 - x^2| \left(\frac{47}{2} x^2 - \frac{13}{2} + \frac{1}{x^2} \right) \\ &\quad + 3(1 - 6x^2 + 4x^4) |\ln x| + \frac{3(1 - 8x^2 + 20x^4)}{\sqrt{4x^2 - 1}} \cos^{-1}\left(\frac{3x^2 - 1}{2x^3}\right). \end{aligned} \quad (51)$$

The NLO QCD and electroweak corrections to the off-shell decays, $h \rightarrow V^* V^* \rightarrow 4\text{-fermions}$, $V = (W, Z)$, are implemented in the public code, PROPHECY4f [28].

4.1.3 $h \rightarrow gg$

The decay of the Higgs boson to gluons only arises through fermion loops in the SM and is sensitive to new colored particles that interact with the Higgs,

$$\Gamma(h \rightarrow gg) = \frac{G_F \alpha_s^2 m_h^3}{64\sqrt{2}\pi^3} \left| \sum_q F_{1/2}(\tau_q) \right|^2, \quad (52)$$

where $\tau_q \equiv 4m_q^2/m_h^2$ and $F_{1/2}(\tau_q)$ is defined to be,

$$F_{1/2}(\tau_q) \equiv -2\tau_q \left[1 + (1 - \tau_q) f(\tau_q) \right]. \quad (53)$$

The function $f(\tau_q)$ is given by,

$$f(\tau_q) = \begin{cases} \left[\sin^{-1}\left(\sqrt{1/\tau_q}\right) \right]^2, & \text{if } \tau_q \geq 1 \\ -\frac{1}{4} \left[\log\left(\frac{x_+}{x_-}\right) - i\pi \right]^2, & \text{if } \tau_q < 1, \end{cases} \quad (54)$$

with

$$x_{\pm} = 1 \pm \sqrt{1 - \tau_q}. \quad (55)$$

In the limit in which the quark mass is much less than the Higgs boson mass,

$$F_{1/2} \rightarrow \frac{2m_q^2}{m_h^2} \log^2\left(\frac{m_q}{m_h}\right). \quad (56)$$

On the other hand, for a heavy quark, $\tau_q \rightarrow \infty$, and $F_{1/2}(\tau_q)$ approaches a constant,

$$F_{1/2} \rightarrow -\frac{4}{3}. \quad (57)$$

Equations (56) and (57) make it clear that the top quark loop is the dominant contribution. QCD corrections to the decay $h \rightarrow gg$ are known at NLO for a finite top quark mass and increase the rate by roughly 60% [29].

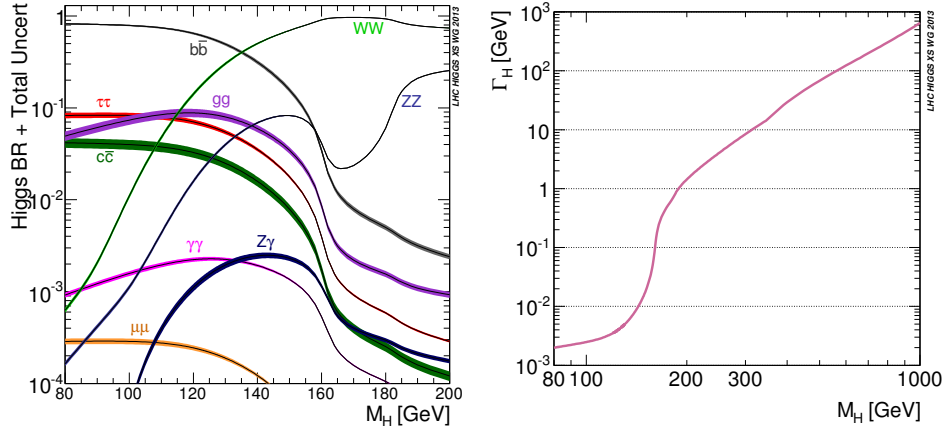


Fig. 3: SM Higgs Branching ratios (LHS) and total width for a SM-like Higgs boson of arbitrary mass (RHS) [22]. In this figure, H is the SM Higgs boson.

4.1.4 $h \rightarrow \gamma\gamma$

The decay $h \rightarrow \gamma\gamma$ arises from fermion and W loops and is an important mode for Higgs measurements at the LHC, despite the smallness of the branching ratio. At lowest order the width is, [5]

$$\Gamma(h \rightarrow \gamma\gamma) = \frac{\alpha^2 G_F}{128\sqrt{2}\pi^3} m_h^3 \left| \sum_i N_{ci} Q_i^2 F_i(\tau_i) \right|^2, \quad (58)$$

where the sum is over fermions and W^\pm bosons with $F_{1/2}(\tau_q)$ given in Equation (53), and

$$F_W(\tau_W) = 2 + 3\tau_W[1 + (2 - \tau_W)f(\tau_W)], \quad (59)$$

with $\tau_W = 4M_W^2/m_h^2$, $N_{ci} = 1(3)$ for leptons (quarks), and Q_i is the electric charge in units of e . In the (unphysical) limit $\tau_W \rightarrow \infty$, $F_W \rightarrow 7$ and we see that the top quark and W contributions have opposite signs. The decay $h \rightarrow \gamma\gamma$ is therefore sensitive to the sign of the top quark Yukawa coupling through the interference of the W and t loops. Similarly, the rate for $h \rightarrow Z\gamma$ receives contributions from both fermions and the W boson. The analytic formula is given in [5] and the $Z\gamma$ width is quite small.

The Higgs branching ratios are shown in Figure 3 for a SM Higgs boson of arbitrary mass [22]. The width of the curves is an estimate of the theoretical uncertainties on the branching ratios. The branching ratios assume SM couplings and no new decay channels and include all known radiative corrections [22]. Also shown in Figure 3 is the Higgs total decay width as a function of Higgs mass. For $m_h = 125 \text{ GeV}$, the total width is very narrow, $\Gamma_h = 4 \text{ MeV}$.

4.2 Higgs Production in Hadronic Collisions

At the LHC, the dominant production mechanisms are gluon fusion, followed by vector boson fusion, shown in Figure 4. The associated production mechanisms of the Higgs with vector bosons or top quarks have smaller rates, but these channels are theoretically important and are shown in Figure 5. It is immediately apparent that gluon fusion and $t\bar{t}h$ production are sensitive to the top quark Yukawa coupling, while vector boson fusion and associated hV , $V = (W, Z)$, production probe the gauge-Higgs couplings.

The total rates for Higgs production in various channels are shown on the LHS of Figure 6 for arbitrary Higgs mass at 13 TeV (LHS) and as a function of center-of-mass energy (RHS) for the physics Higgs mass. The curves include the most up-to-date theoretical calculations, and the width of the curves represents an estimate of the uncertainties [30]. We will discuss each production channel in turn in this section.

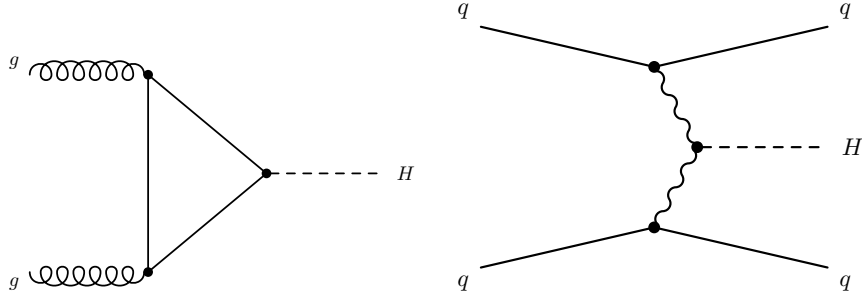


Fig. 4: Contribution to Higgs boson production from (LHS) gluon fusion and (RHS) vector boson scattering. In this figure, H is the SM Higgs boson.

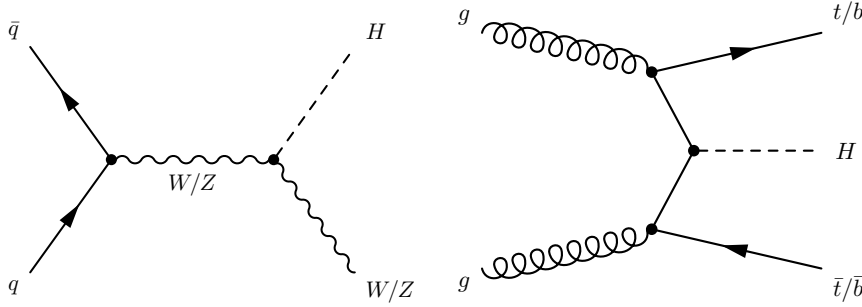


Fig. 5: Contribution to Higgs boson production from (LHS) associated Vh production and (RHS) $t\bar{t}h$ production. In this figure, H is the SM Higgs boson.

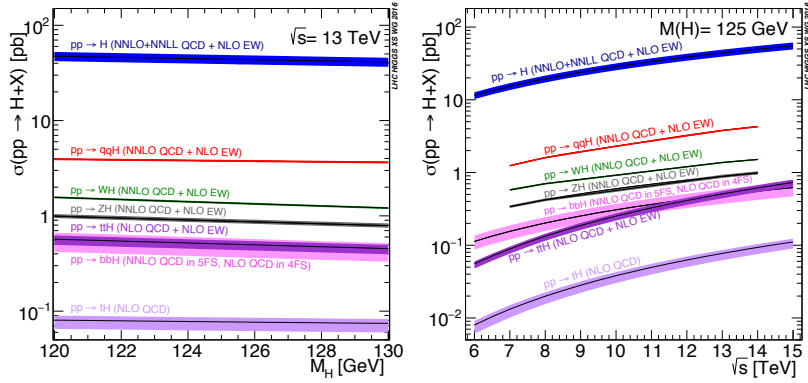


Fig. 6: Total Higgs production cross sections [30]. In this figure, H is the SM Higgs boson.

4.2.1 $gg \rightarrow h$

The primary production mechanism for a Higgs boson in hadronic collisions is through the couplings to heavy fermions, $gg \rightarrow h$, which is shown on the LHS of Figure 4. This process is dominated by the top quark loop and the loop with a bottom quark contributes roughly -5% to the SM cross section.

The lowest order (LO) amplitude for $g^{A,\mu}(p) + g^{B,\nu}(q) \rightarrow h$ from a quark of mass m_q in the loop is,

$$A^{\mu\nu}(g^A g^B \rightarrow h) = \frac{\alpha_s}{4\pi v} \delta_{AB} \left(g^{\mu\nu} \frac{m_h^2}{2} - p^\nu q^\mu \right) F_{1/2}(\tau_q) \epsilon_\mu(p) \epsilon_\nu(q)$$

$$\rightarrow -\frac{\alpha_s}{3\pi v}\delta_{AB}\left(g^{\mu\nu}\frac{m_h^2}{2}-p^\nu q^\mu\right)\epsilon_\mu(p)\epsilon_\nu(q) \quad \text{if } m_q \gg m_h. \quad (60)$$

The partonic cross section can be found from the general resonance formula,

$$\hat{\sigma}(gg \rightarrow h) = \frac{16\pi^2}{m_h}(2J+1)\frac{1}{64} \cdot \frac{1}{4} \cdot 2\Gamma(h \rightarrow gg)\delta(s-m_h^2), \quad (61)$$

where the factors of $\frac{1}{64}$ and $\frac{1}{4}$ are the color and spin averages, $J=0$ is the Higgs spin, s is the gg partonic sub-energy, and the factor of 2 undoes the identical particle factor of $\frac{1}{2}$ in the decay width $\Gamma(h \rightarrow gg)$. The lowest order partonic cross section for $gg \rightarrow h$ is,

$$\begin{aligned} \hat{\sigma}(gg \rightarrow h) &= \frac{\alpha_s^2}{1024\pi v^2} \left| \sum_q F_{1/2}(\tau_q) \right|^2 \delta\left(1 - \frac{s}{m_h^2}\right) \\ &\equiv \hat{\sigma}_0(gg \rightarrow h)\delta\left(1 - \frac{s}{m_h^2}\right). \end{aligned} \quad (62)$$

In the heavy quark limit, the cross section is independent of the top quark mass and becomes a constant,

$$\hat{\sigma}_0(gg \rightarrow h) \sim \frac{\alpha_s^2}{576\pi v^2}. \quad (63)$$

The heavy fermions do not decouple at high energy and the gluon fusion rate essentially counts the number of SM-like chiral quarks.

The Higgs boson production cross section at a hadron collider can be found by integrating the partonic cross section, $\sigma_0(pp \rightarrow h)$, with the gluon parton distribution functions, $g(x, \mu)$,

$$\sigma(pp \rightarrow h) = \hat{\sigma}_0 z \int_z^1 \frac{dx}{x} g(x, \mu) g\left(\frac{z}{x}, \mu\right), \quad (64)$$

where σ_0 is given in Equation (62), $z \equiv m_h^2/S$, μ is the factorization scale and S is the hadronic center of mass energy. It is particularly interesting to consider the theoretical accuracy at N^3LO [31],

$$\sigma(pp \rightarrow h)[13 \text{ TeV}] = 48.58_{-6.7\%}^{+4.6\%}(\text{theory}) \pm 3.2\%(\text{PDF} + \alpha_s), \quad (65)$$

where the theory uncertainty arises predominantly from the scale choice and the PDF+ α_s uncertainty is the PDF and correlated uncertainty on α_s .

The measured Higgs rate immediately rules out the possibility of a 4th generation of SM chiral fermions. Imagine that there are heavy fermions, \mathcal{T} and \mathcal{B} , with identical quantum numbers as the SM top and bottom quarks. The new fermions would contribute to Higgs production from gluon fusion as on the LHS of Figure 4. From Equation (63), we would have,

$$\begin{aligned} \hat{\sigma}_0(gg \rightarrow h) &\rightarrow \frac{\alpha_s^2}{576\pi v^2} \left[1 + 1 + 1\right]^2 \\ &\rightarrow 9\hat{\sigma}_0(SM), \end{aligned} \quad (66)$$

where the factors in the square bracket represent the contributions of the SM t , \mathcal{T} and \mathcal{B} . This is obviously excluded by the measured rate for gluon fusion Higgs production, which is in good agreement with the SM prediction.

The tensor structure of Equation (60) is exactly that required for the production of a spin-0 particle from 2-gluons with momentum, $g(k_1)$ and $g(k_2)$. Starting from a $G_{\mu\nu}G^{\mu\nu}$ term in the Lagrangian and considering only the Abelian contributions for now,

$$G_{\mu\nu}G^{\mu\nu} \rightarrow (\partial_\mu G_\nu - \partial_\nu G_\mu)(\partial^\mu G^\nu - \partial^\nu G^\mu). \quad (67)$$

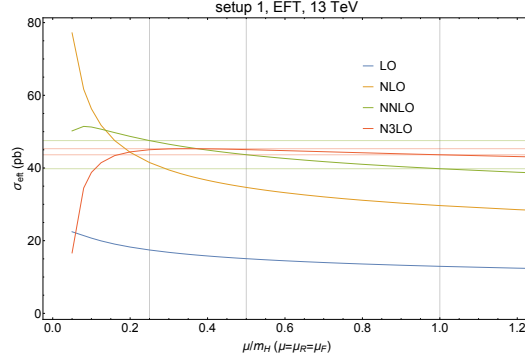


Fig. 7: QCD corrected rate for gluon fusion as a function of the factorization and renormalization scale [31].

Making the replacement $\partial_\mu \rightarrow ik_\mu$,

$$\begin{aligned}
 G_{\mu\nu}G^{\mu\nu} &\rightarrow -(k_{1\mu}G_{1\nu} - k_{1\nu}G_{1\mu})(k_2^\mu G_2^\nu - k_2^\nu G_2^\mu) \\
 &= -2\left(k_1 \cdot k_2 G_1 \cdot G_2 - k_1 \cdot G_2 k_2 \cdot G_1\right) \\
 &= -2k_1 \cdot k_2 G_{1\mu} G_{2\nu} \left[g^{\mu\nu} - \frac{k_1^\nu k_2^\mu}{k_1 \cdot k_2} \right].
 \end{aligned} \tag{68}$$

Comparing Equations (60) and (68)⁷ suggests that the heavy quark limit for the gluon fusion production of a Higgs boson can be obtained from the effective dimension-5 Lagrangian

$$L_{EFT} = \frac{\alpha_s}{12\pi} \frac{h}{v} G_{\mu\nu}^A G^{\mu\nu A}. \tag{69}$$

The effective Lagrangian of Equation (69) has been used to calculate the QCD corrections to gluon fusion to NLO, NNLO, and N³LO [31]. The result is shown in Figure 7. Note that there is a large correction (approximately a factor of 2) going from LO to NLO. The corrections at each order remain sizable and the dependence on the factorization scale, μ is reduced at higher order.

4.2.2 p_T distribution of Higgs Bosons

At LO, the Higgs boson has no p_T and a transverse momentum spectrum for the Higgs is first generated by the process, $gg \rightarrow gh$, which is an NLO contribution to the gluon fusion process [32]. As $p_T \rightarrow 0$, the partonic cross section for Higgs plus jet production diverges as $1/p_T^2$,

$$\begin{aligned}
 \frac{d\hat{\sigma}}{dt}(gg \rightarrow gh) &= \hat{\sigma}_0 \frac{3\alpha_s}{2\pi} \left\{ \frac{1}{p_T^2} \left[\left(1 - \frac{m_h^2}{s}\right)^4 + 1 + \left(\frac{m_h^2}{s}\right)^4 \right] \right. \\
 &\quad \left. - \frac{4}{s} \left(1 - \frac{m_h^2}{s}\right)^2 + \frac{2p_T^2}{s} \right\},
 \end{aligned} \tag{70}$$

where $\hat{\sigma}_0$ is the LO $gg \rightarrow h$ cross section given in Equation (62), and s, t and u are the partonic Mandelstam invariants. The p_T spectrum for Higgs plus jet at LO is shown in Figure 8, where the contributions from the gg and $qg, \bar{q}g$ initial states are shown separately. Also shown is the $m_t \rightarrow \infty$ limit of the spectrum that is derived from the effective Lagrangian of Equation (69). The effective Lagrangian approximation fails around $p_T \sim 2m_t$. In this process, there are several distinct momentum scales (p_T, m_h, m_t), as opposed to gluon fusion where there is only a single scale (m_h/m_t) at LO. The

⁷The extra factor of $\frac{1}{2}$ comes from the neglected color factor, $\text{Tr}(T^A T^B) = \frac{1}{2} \delta_{AB}$.

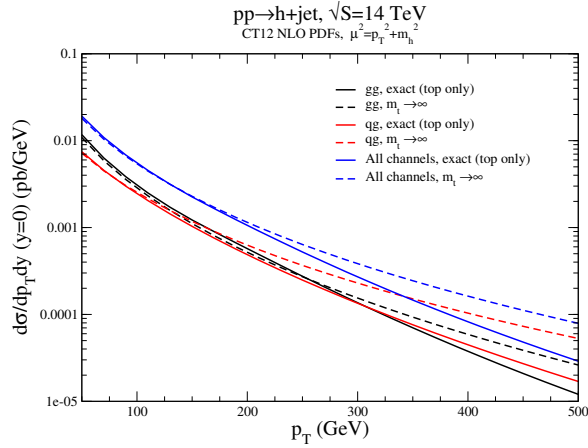


Fig. 8: Lowest order p_T spectrum for Higgs plus jet production from Equation (70) and the large m_t approximation of Equation (69).

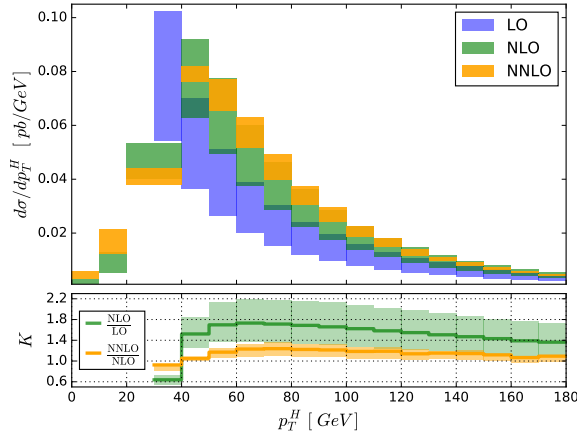


Fig. 9: QCD corrected p_T spectrum for Higgs plus jet production at $\sqrt{S} = 8 \text{ TeV}$ [33,34]. In this figure, H is the SM Higgs boson.

expansion in $\frac{m_h}{m_t}$ for $gg \rightarrow gh$ receives corrections of $\mathcal{O}\left(\frac{s}{m_t^2}, \frac{p_T^2}{m_t^2}\right)$ and for $p_T \gtrsim 2m_t$, the EFT large top quark mass expansion cannot be used to obtain reliable distributions.

NLO, NNLO, and N³LO radiative corrections to Higgs plus jet production have been calculated [33–36] using the $m_t \rightarrow \infty$ approximation. The lowest order result of Equation (70) is then reweighted by a K factor derived in the $m_t \rightarrow \infty$ limit for each kinematic bin. The effects of the higher order corrections are significant and increase the rate by a factor of around 1.8 as shown in Figure 9. The singularity of the LO result at $p_T = 0$ is clearly visible in Figure 9 and we note that after the inclusion of the NLO corrections, the p_T spectrum no longer diverges as $p_T \rightarrow 0$.

The terms which are singular as $p_T \rightarrow 0$ can be isolated and the integrals performed explicitly. Considering only the gg initial state [37],

$$\frac{d\sigma}{dp_T^2 dy}(pp \rightarrow gh) \Big|_{p_T^2 \rightarrow 0} \sim \hat{\sigma}_0 \frac{3\alpha_s}{2\pi} \frac{1}{p_T^2} \left[6 \log\left(\frac{m_h^2}{p_T^2}\right) - 2\beta_0 \right] g(ze^y)g(ze^{-y}) + \dots \quad (71)$$

where $z \equiv m_h^2/S$, $\beta_0 = (33 - 2n_{lf})/6$, and $n_{lf} = 5$ is the number of light flavors. Clearly when $p_T \ll m_h$, the terms containing the logarithms resulting from soft gluon emission can give a large

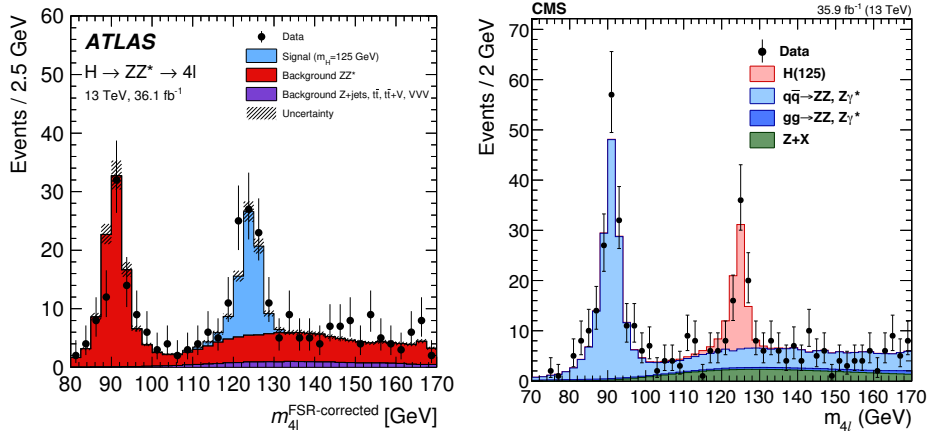


Fig. 10: $h \rightarrow ZZ \rightarrow 4$ lepton signal at 13 TeV [40, 41].



Fig. 11: Contributions to $gg \rightarrow ZZ \rightarrow 4l$. The dominant contributions to the triangle and box diagrams are from the top quark.

numerical contribution. The logarithms of the form $\alpha_s^n \log^m(m_h^2/p_T^2)$ can be resummed [37, 38] to improve the theoretical accuracy in the regime $p_T \rightarrow 0$ [39].

4.2.3 Measuring the Higgs width with $gg \rightarrow h \rightarrow ZZ$

Gluon fusion with the subsequent Higgs decay to $ZZ \rightarrow 4$ leptons or $\gamma\gamma$ were the Higgs discovery channels. The $h \rightarrow ZZ \rightarrow 4$ lepton signals at 13 TeV are shown in Figure 10 [40, 41] and the Higgs resonance is clearly visible. Making a direct measurement of the Higgs width by fitting a Breit-Wigner function to the resonance shape is not possible since the detector resolution is $\mathcal{O}(1 - 2) GeV$, much larger than the Higgs width, $\Gamma_h \sim 4 MeV$.

A clever idea uses the properties of the longitudinal Z polarizations [42, 43]. Consider the process $gg \rightarrow ZZ \rightarrow 4l$ shown in Figure 11. The Higgs contribution is shown on the LHS of Figure 11 and the partonic cross section from the Higgs contribution alone is generically given by,

$$\hat{\sigma}(gg \rightarrow h \rightarrow ZZ) \sim \int ds \frac{|A(gg \rightarrow h)|^2 |A(h \rightarrow ZZ)|^2}{(s - m_h^2)^2 + \Gamma_h^2 m_h^2}. \quad (72)$$

We allow the effective $gg \rightarrow h$ and $h \rightarrow ZZ$ couplings to be scaled from the SM values by arbitrary factors $\kappa_g(s)$ and $\kappa_Z(s)$, where we explicitly note that the κ factors can in principle depend on scale,

$$|A(gg \rightarrow h)|^2 |A(h \rightarrow ZZ)|^2 \sim \kappa_g^2(s) \kappa_Z^2(s) |\epsilon_{Z1} \cdot \epsilon_{Z2}|^2, \quad (73)$$

where ϵ_{Zi}^μ are the Z polarization vectors.

The interesting observation is that Equation (72) behaves very differently above the Higgs reso-

nance and near the resonance. Above the resonance, $s \gg m_h^2$, Equation (72) becomes,

$$\hat{\sigma}(gg \rightarrow h \rightarrow ZZ)^{above} \sim \int ds \frac{\kappa_g^2(s) \kappa_Z^2(s) |\epsilon_{Z1} \cdot \epsilon_{Z2}|^2}{s^2}. \quad (74)$$

For transverse polarizations, nothing particularly interesting happens, but because of the electroweak symmetry breaking the longitudinally polarized Z bosons have a novel feature. Defining the momenta of the outgoing Z bosons as p_{Z1} and p_{Z2} and remembering that the longitudinal polarization is approximately given by,

$$\epsilon_L^\mu(p_Z) \sim \frac{p_Z^\mu}{M_Z} + \mathcal{O}\left(\frac{M_Z^2}{s}\right), \quad (75)$$

we observe that $\epsilon_L \cdot \epsilon_L \sim \frac{p_{Z1} \cdot p_{Z2}}{M_Z^2} \sim \frac{s}{M_Z^2}$. Equation (74) has the approximate form for $s \gg m_h^2$,

$$\hat{\sigma}(gg \rightarrow h \rightarrow Z_L Z_L)^{above} \sim \int ds \frac{\kappa_g^2(s) \kappa_Z^2(s)}{M_Z^4}. \quad (76)$$

We note that Equation (76) exhibits no dependence on the Higgs width.

Near the Higgs resonance, we can use the narrow width approximation, which amounts to the replacement,

$$\frac{1}{(s - m_h^2)^2 + (m_h \Gamma_h)^2} \rightarrow \frac{\pi}{m_h \Gamma_h} \delta(s - m_h^2) \quad (77)$$

and Equation (72) is approximately,

$$\hat{\sigma}(gg \rightarrow h \rightarrow ZZ)^{on} \sim \frac{\kappa_g^2(m_h^2) \kappa_Z^2(m_h^2)}{m_h \Gamma_h}. \quad (78)$$

The idea is that by measuring the $gg \rightarrow h \rightarrow ZZ$ rate above and on the resonance, information can be extracted about the Higgs width. Assuming the κ factors do not depend on scale,

$$\Gamma_h \sim \frac{\hat{\sigma}^{above}}{\hat{\sigma}^{on}}. \quad (79)$$

At 8 TeV , approximately 15% of the cross section has $m_{4l} > 140 GeV$, so this is a promising idea. If the κ factors have an energy dependence, they do not cancel in Equation (79) and the interpretation of the measurement becomes more complicated.

Of course, a real calculation needs to include both the diagrams of Figure 11, along with the interference, and this has been done by several groups with results shown in Figure 12. The importance of including the interference terms is apparent, but the long tail at high m_{4l} (shown in red) is clear. ATLAS and CMS have used this technique to place limits on the Higgs width [44, 45],

$$\Gamma_h \lesssim (4 - 5) \Gamma_h^{SM}. \quad (80)$$

There are some big assumptions in this extraction of the Higgs width, the most obvious of which is the assumption that the κ factors are the same on and off the Higgs resonance peak. This is clearly a false assumption, since in a quantum field theory all couplings run. If there are anomalous hZZ (or hgg) couplings, than the running could be changed significantly [46, 47]. For example, a contribution to the EFT of the form,

$$L \sim \frac{c_Z}{\Lambda^2} \frac{h}{v} Z_{\mu\nu} Z^{\mu\nu} \quad (81)$$

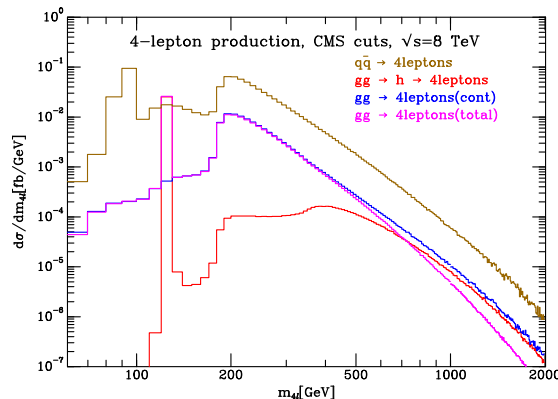


Fig. 12: Contributions to $gg \rightarrow ZZ \rightarrow 4l$ at 8 TeV. The Higgs contributions are shown in red, while the total rate from gluon fusion including interference is given in magenta [49].

would give contributions of $\mathcal{O}\left(\frac{s}{\Lambda^2}\right)$ and would cause m_{4l} to grow above the peak, and would invalidate the extraction of Γ_h . Additional colored particles in the ggh loop would also change the interpretation of the $gg \rightarrow ZZ \rightarrow 4$ lepton result as a measurement of the Higgs width [48].

It is worth noting that an e^+e^- collider with an energy of $\sqrt{s} = 500$ GeV can make a 5% measurement of Γ_h with an integrated luminosity of 500 GeV [50]. First the measurement of $e^+e^- \rightarrow Zh$ is made by tagging the Zh events where the recoil mass is consistent with a Higgs boson. This is done using conservation of momenta and determines $\sigma(Zh)$. Next we can measure the $h \rightarrow ZZ$ rate to determine $BR(h \rightarrow ZZ)$. The Higgs width is then determined in a model independent fashion,

$$\begin{aligned} \Gamma_h &= \Gamma(h \rightarrow ZZ)BR(h \rightarrow ZZ) \\ &\sim \frac{\sigma(Zh)}{BR(h \rightarrow ZZ)}. \end{aligned} \quad (82)$$

4.2.4 Vector Boson Scattering

The vector boson scattering (VBS) process is shown on the RHS of Figure 4. It can be thought of as 2 incoming quarks each radiating a W or Z boson, which then form a Higgs. Vector boson fusion also offers the opportunity to observe the $2 \rightarrow 2$ scattering process, $VV \rightarrow VV$, ($V = Z, W$), which is extremely sensitive to new physics in the electroweak sector. The $VV \rightarrow VV$ sub-process plays a special role in Higgs physics since the Higgs exchange contributions unitarize the scattering amplitude.

VBS production of a Higgs occurs through the purely electroweak process $q\bar{q}' \rightarrow q\bar{q}'h$ which has a distinctive experimental signature and vanishes in the limit $v = 0$. The outgoing jets are peaked in the forward and backward regions and can be used to tag the VBF event. This can easily be seen by considering the top leg of the RHS of Figure 4:

$$q(p) \rightarrow q'(p')V(k). \quad (83)$$

In the lab frame,

$$\begin{aligned} p &\equiv E(1, 0, 0, 1) \\ p' &\equiv E'(1, 0, \sin \theta, \cos \theta). \end{aligned} \quad (84)$$

The integral over the final state phase space for the VBS scattering cross section has a generic contribution,

$$\sigma \sim \int \frac{(\text{Phase Space})}{[(p - p')^2 - M_V^2]^2} \sim \int \frac{\theta d\theta}{[2EE'(1 - \cos \theta) - M_V^2]^2} \sim \int \frac{\theta d\theta}{[\theta^2 - M_V^2/EE']^2} \quad (85)$$

which is enhanced in the $\theta \rightarrow 0$ region for $E, E' \gg M_V^2$. In addition, these forward tagging jets have a large invariant mass and small p_T . Typical cuts on the jets are,

$$p_{T_j} > 20 \text{ GeV}, |y_j| < 5, |y_{j_1} - y_{j_2}| > 3, M_{jj} > 130 \text{ GeV}. \quad (86)$$

The decay products from the intermediate VV scattering are mostly contained in the central rapidity region. These characteristics can be used to separate VBS scattering from QCD gluon initiated events and the non-VBS contributions can be suppressed to $\sim 1 - 2\%$ [51]. The ability to separate the Higgs signal into gluon initiated events and VBF events is crucial for the extraction of Higgs coupling constants.

4.2.5 Associated Production

At the LHC the process $q\bar{q} \rightarrow Vh$ offers the hope of being able to tag the Higgs boson by the V boson decay products [52], although as shown in Figure 6 the rate is significantly smaller than the dominant $gg \rightarrow h$ production mechanism. The cross section for Wh production is,

$$\hat{\sigma}(q_i\bar{q}_j \rightarrow W^\pm h) = \frac{G_F^2 M_W^6 |V_{ij}|^2}{6\pi s^2 (1 - M_W^2/s)^2} \lambda_{Wh}^{1/2} \left[1 + \frac{s\lambda_{Wh}}{12M_W^2} \right], \quad (87)$$

where $\lambda_{Wh} = 1 - 2(M_W^2 + m_h^2)/s + (M_W^2 - m_h^2)^2/s^2$ and V_{ij} is the CKM angle associated with the $q_i\bar{q}_j W$ vertex. The rate for Zh is about a factor of 3 smaller than that for Wh and analytic results can be found in Ref. [4]. The NNLO QCD and NLO electroweak corrections are known, so there is relatively little uncertainty on the prediction [53, 54].

The Vh associated channel has recently been used to observe the decay $h \rightarrow b\bar{b}$ [55, 56], using the jet substructure techniques first proposed in Ref. [57]. The idea is that by going to high transverse momentum for the Higgs, the backgrounds can be significantly reduced. Jet substructure techniques are discussed in the lectures of Schwartz at this school [58].

4.2.6 $t\bar{t}h$ Production

The top quark Yukawa coupling, Y_t , can be directly measured in the $t\bar{t}h$ process shown on the RHS of Figure 5. Recall that the gluon fusion production of the Higgs is also proportional to the top quark Yukawa, but in addition it can receive enhanced contributions from the bottom quark Yukawa interactions in some BSM scenarios, along with contributions from new colored scalars. The NLO QCD [59–62] and electroweak corrections [63, 64] for $t\bar{t}h$ production are known and contribute to very precise predictions [30]:

$$\begin{aligned} \sqrt{S} = 8 \text{ TeV} & & \sigma_{t\bar{t}h} = .133 \text{ pb}_{-9\%}^{+4\%}(\text{scale}) \pm 4.3\%(PDF + \alpha_s) \\ \sqrt{S} = 13 \text{ TeV} & & \sigma_{t\bar{t}h} = .507 \text{ pb}_{-9.2\%}^{+5.8\%}(\text{scale}) \pm 3.6\%(PDF + \alpha_s). \end{aligned} \quad (88)$$

Although numerically small, electroweak corrections spoil the direct proportionality of the lowest order cross section to Y_t^2 .

This process has large backgrounds from $t\bar{t}b\bar{b}$ and $t\bar{t}jj$. In order to suppress the backgrounds, many $t\bar{t}h$ searches are done in the boosted regime, where the electroweak Sudakov logarithms become relevant. A definitive measurement of this channel has not yet been made, and will be one of the important milestones of the coming LHC run.

The associated production of $b\bar{b}h$ is not relevant in the SM, but can be important in models with enhanced b Yukawa couplings.

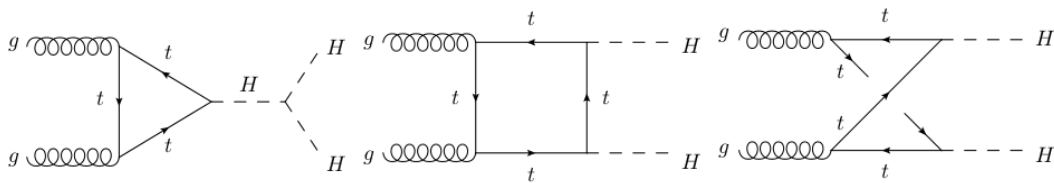


Fig. 13: Contributions to $gg \rightarrow hh$ in the SM. The dominant contribution to the triangle and box diagrams are from the top quark. In this figure, H is the SM Higgs boson.

4.2.7 Double Higgs Production

Finally, we need to measure the parameters of the Higgs potential, Equation (30), to determine if electroweak symmetry breaking really proceeds as in the SM. In the SM, the Higgs potential is,

$$V = \frac{m_h^2}{2} h^2 + \lambda_3 h^3 + \lambda_4 h^4, \quad (89)$$

where $\lambda_3^{SM} = m_h^2/(2v)$ and $\lambda_4^{SM} = h^2/(8v^2)$. It is apparent that the Higgs self-couplings are weak,

$$\lambda_3^{SM} = .13v, \quad \lambda_4^{SM} = .03. \quad (90)$$

The only way to directly probe the h^3 coupling is by double Higgs production and the dominant production mechanism is gluon fusion as shown in Figure 16. The result is sensitive to new colored particles running in the loops, along with modifications to the Higgs tri-linear self-coupling and the top quark Yukawa coupling (Equations (89) and (26)).

The large m_t limit has been used to compute QCD corrections to NLO [65] and NNLO [66]. In this approach, a K factor is computed:

$$K \equiv \frac{d\sigma_{NNLO}}{d\sigma_{LO}}, \quad (91)$$

where the distributions in Equation (91) are computed in the $m_t \rightarrow \infty$ limit and are then used to rescale the lowest order distributions computed with finite m_t ⁸ [67–70]. The exact NLO result for double Higgs production including all top mass effects is now known and can be used to obtain distributions [71, 72]. The effects of including the top quark mass exactly at NLO are significant and reduce the total cross section by $\sim 14\%$ at $14 TeV$ from the B.i. NLO HEFT limit. Including the top quark mass effects also has significant effects on distributions, as demonstrated in Figure 15.

The dependence of hh production on λ_3 from various production mechanisms is shown in Figure 16 [73] as a function of $\delta_3 \equiv \frac{\lambda_3}{\lambda_3^{SM}}$.⁹

The best current limits from the $8 TeV$ data on double Higgs production are,

$$\begin{aligned} \frac{\sigma(pp \rightarrow hh)}{\sigma(pp \rightarrow hh)|_{SM}} &< 29 && \text{ATLAS,} \\ \frac{\sigma(pp \rightarrow hh)}{\sigma(pp \rightarrow hh)|_{SM}} &< 19 && \text{CMS,} \end{aligned} \quad (92)$$

which still leaves a way to go before we get to an interesting regime. The ATLAS limit is from the $b\bar{b}b\bar{b}$ final state [74], while the CMS limit is from the $b\bar{b}\gamma\gamma$ final state [75]. ATLAS estimates that a luminosity of $3 ab^{-1}$ will be sensitive to $\delta_3 > 8.7$ and $\delta_3 < -1.3$ [76]. This is clearly not the precision measurement we desire and the need to measure the Higgs tri-linear coupling is one of the major motivations for a $100 TeV$ collider.

⁸This is termed the B.i. NLO HEFT in Figure 15.

⁹The curve labelled EFT loop-improved is identical to the B.i. NLO HEFT approximation.

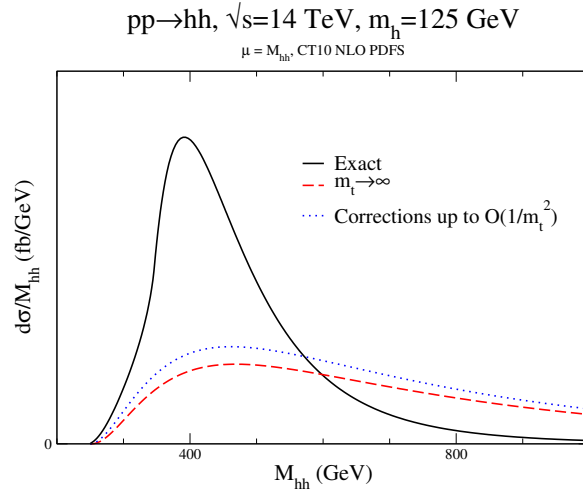


Fig. 14: LO transverse momentum distribution for double Higgs production in the SM, compared with the large m_t limit, along with the first correction of $\mathcal{O}(s/m_t^2)$.

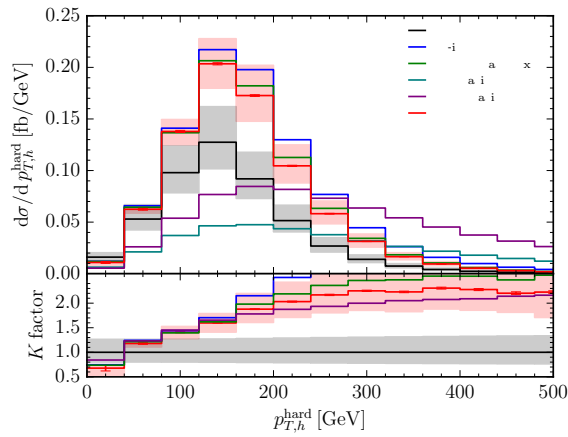


Fig. 15: Transverse momentum distribution for double Higgs production in the SM, including various approximations for the QCD corrections. The curve labelled NLO includes all finite m_t effects [72].

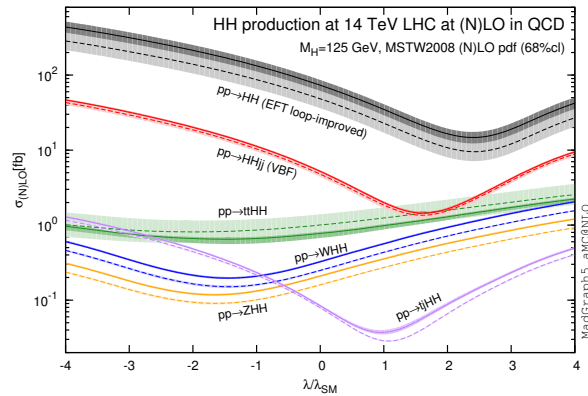


Fig. 16: Dependence of double Higgs production rates on the Higgs tri-linear self-coupling [73].

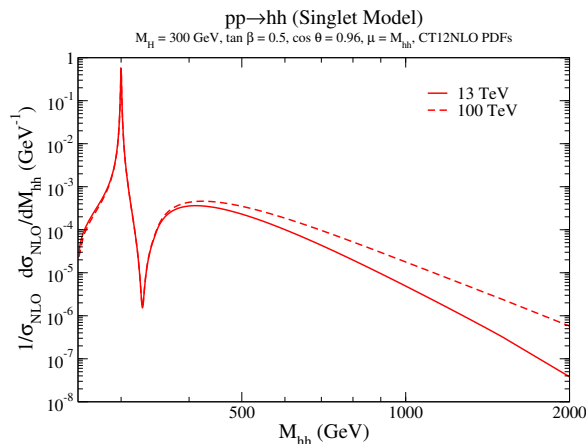


Fig. 17: Double Higgs production in the Z_2 symmetric singlet model with a heavy neutral scalar of mass $M_H = 300$ GeV [77].

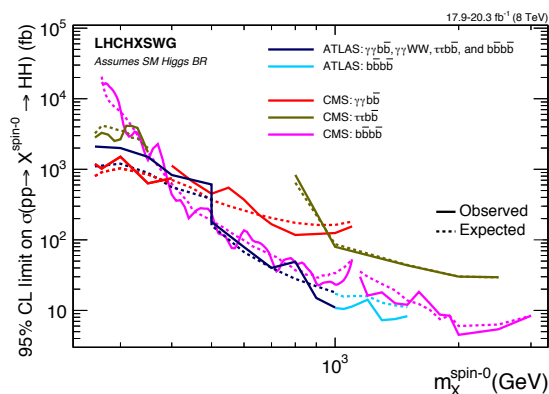


Fig. 18: Experimental limits from the LHC on hh production in a BSM theory containing an s -channel scalar resonance with mass M_X [30].

The fact that the SM rate for double Higgs production is quite small makes it an ideal place to search for new physics. Many models (singlet, 2HDM, MSSM, NMSSM, etc) [77–81] contain heavy neutral scalars that can decay into 2 SM Higgs bosons with a significant ($\sim 30\%$) branching ratio. In these models, there is an s -channel resonance from the heavy Higgs particle, and there will be interference between this new scalar and the SM Higgs giving the classic dip structure shown in Figure 17 for the example of the singlet model. Limits on resonant decays in the generic BSM process, $gg \rightarrow X \rightarrow hh$ for various final states are shown in Figure 18, where for heavy resonances, the most important search channel is the $4b$ final state.

It has been proposed that indirect limits on λ_3 may be extracted from the dependence of electroweak radiative corrections to single Higgs production on the Higgs tri-linear coupling. This coupling enters the rate for $gg \rightarrow h$ at 2-loops and contributes to the $t\bar{t}h$, Vh , and VBS processes at 1-loop. Of course λ_3 is not a free parameter in the SM, and some care must be taken with the renormalization prescription. Ref. [82] obtains the allowed 2σ region from a fit to single Higgs production,

$$-9.4 < \delta_3 < 16. \quad (93)$$

Similar allowed regions are obtained in Refs. [83–85]. The allowed parameter space from current fits to single Higgs production are not significantly different from the expected limits on λ_3 with $3 ab^{-1}$ at the LHC.

5 Effective Field Theory and the Higgs Boson

5.1 Higgs Boson Coupling measurements

The production of the Higgs boson in Run-I at the LHC produced results which basically agree with the SM predictions at the 10 – 20% level [86]. Preliminary Higgs coupling results at 13 TeV [56, 87–91], are also in reasonable agreement with expectations. The rates are as predicted, and there are no non-SM like light (EW scale) particles observed.

What we need is a way to quantify small deviations from the SM predictions. The simplest way is to introduce an arbitrary scaling into the SM interactions,

$$L_\kappa = \sum_f \kappa_f \frac{m_f}{v} \bar{f} f h + \kappa_W g M_W W^{+\mu} W_\mu^- h + \kappa_Z g \frac{M_Z}{c_W} Z^\mu Z_\mu h. \quad (94)$$

In the SM, all κ parameters are 1, so a deviation would indicate some physics not contained in the SM. Of course, Equation (94) is not $SU(2)_L \times U(1)_Y$ gauge invariant, but it serves as a starting point for study.

For a given production and decay channel, $i \rightarrow h \rightarrow j$,

$$\begin{aligned} \kappa_i^2 &= \frac{\sigma(i \rightarrow h)}{\sigma(i \rightarrow h)_{SM}} \\ \kappa_j^2 &= \frac{\Gamma(h \rightarrow j)}{\Gamma(h \rightarrow j)_{SM}}. \end{aligned} \quad (95)$$

The κ formalism also rescales the total width,

$$\begin{aligned} \kappa_h &\equiv \frac{\Gamma_h}{\Gamma_h^{SM}} \\ \Gamma_h &= \sum_X \kappa_X^2 \Gamma(h \rightarrow XX) + \Gamma(h \rightarrow \text{invisible}), \end{aligned} \quad (96)$$

where $\Gamma(h \rightarrow \text{invisible})$ is any unobserved decay. This approach assumes that there are no new light resonances, no new tensor structures in the Higgs interactions beyond those of the SM, that the narrow width approximation for Higgs decays is valid, and is based on rescaling total rates (that is, no new dynamics is included).

A combined CMS/ATLAS fit is shown in Figure 19. This particular fit does not allow for new physics in the $gg \rightarrow h$ and $h \rightarrow \gamma\gamma$ channels, but instead parameterizes the effective couplings in terms of the SM interactions of the Higgs with the top and bottom (κ_g) and with the W and top (κ_γ) as,

$$\begin{aligned} \kappa_g^2 &\sim 1.06\kappa_t^2 + .01\kappa_b^2 - .07\kappa_t\kappa_b \\ \kappa_\gamma^2 &\sim 1.59\kappa_W^2 + .07\kappa_t^2 - .66\kappa_W\kappa_t. \end{aligned} \quad (97)$$

Similar results are shown in Figure 20, and again the results are in general agreement with the SM predictions. With the addition of 13 TeV data, the Higgs couplings should become even more constrained. In particular, the tth and bbh coupling measurements have been significantly updated from Figure 20.

ATLAS and CMS have various types of fits. In some fits, they separate Higgs bosons from different production and decay channels. Other fits allow for unobserved decay channels, or new contributions to gluon fusion or the decay to $\gamma\gamma$. None of the fits show any significant deviation from the SM predictions.

Finally, a fit to all Higgs production and decay channels yields the combined ATLAS/CMS result [86],

$$\mu \equiv \frac{\sigma_h}{\sigma_h(SM)} = 1.0 \pm 0.07(stat) \pm 0.04(syst) \pm 0.03(theory). \quad (98)$$

From Equation (98), it is clear that the accuracy of the theoretical predictions will soon be the limiting factor in the interpretation of Higgs measurements.

To improve on the fits to total rates, we need to construct an effective field theory, which is the topic of the next section.

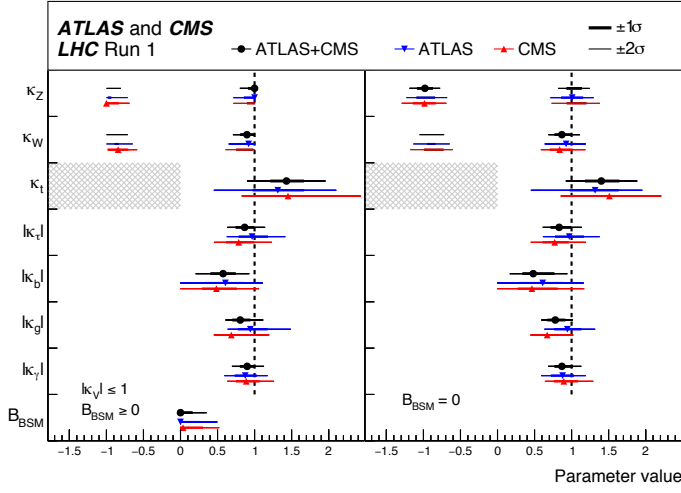


Fig. 19: Combined ATLAS/CMS κ fits to Run-1 data [86].

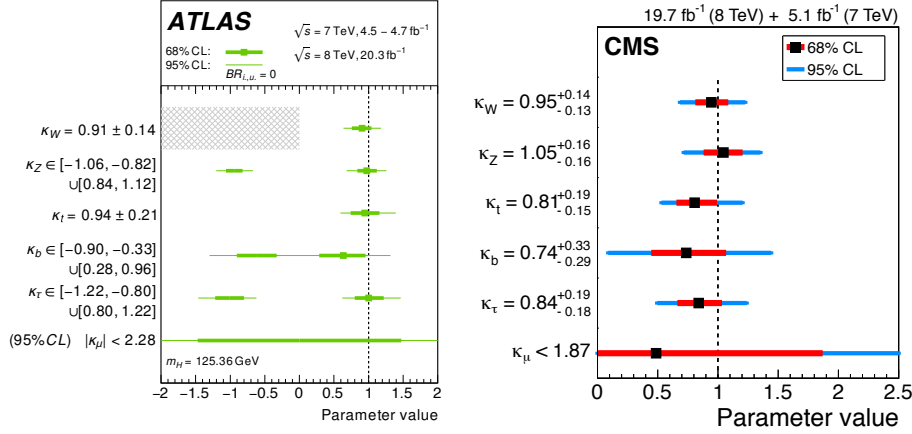


Fig. 20: ATLAS κ fits to Run-1 data [92] (LHS) and CMS κ fits to Run-1 data [93] (RHS).

5.2 Effective Field Theory Basics

The effective field theory (EFT) Lagrangian we use assumes that there are no new light degrees of freedom and is constructed by writing an $SU(2)_L \times U(1)_Y$ invariant Lagrangian as an expansion in powers of v/Λ , where Λ is some high scale where we envision that there is a UV complete theory [94, 103],

$$L_{EFT} = L_{SM} + \sum_i \frac{c_i^5}{\Lambda} O_i^5 + \sum_i \frac{c_i^6}{\Lambda^2} O_i^6 + \dots \quad (99)$$

and O_i^n is a dimension- n operator constructed from SM fields. The EFT allows for a systematic study of BSM physics effects in a gauge invariant fashion and radiative corrections can be implemented order by order in $\frac{v}{\Lambda}$.

The only possible dimension-5 operator violates lepton number conservation and is typically neglected in studies of Higgs physics. There are many possible bases for constructing the dimension-6 operators, of which the most well-known are the Warsaw [95], HISZ [96], and SILH [97] bases. By using the equations of motion, there is a mapping from one basis to the next [98, 99]. Note that the HISZ basis does not contain fermion interactions.

There are several approaches to using the dimension-6 truncation of the EFT of Equation (99). One could calculate an amplitude to $\mathcal{O}\left(\frac{v^2}{\Lambda^2}\right)$,

$$A \sim A_{SM} + \frac{A_{EFT}^6}{\Lambda^2}. \quad (100)$$

Squaring the amplitude,

$$|A|^2 \sim \left| A_{SM} + \frac{A_{EFT}^6}{\Lambda^2} \right|^2, \quad (101)$$

we obtain results that are guaranteed to be positive-definite. The problem is that Equation (101) contains terms $\sim \frac{(A_{EFT}^6)^2}{\Lambda^4}$ that are of the same order in v^2/Λ^2 as the neglected dimension-8 terms. The expansion only makes sense if

$$|A_{EFT}^6|^2 \ll |A_{SM}^* A_{EFT}^8|, \quad (102)$$

which can be arranged in some BSM models [100].

We begin by considering a simple EFT with just 2 non-SM terms,

$$L \sim L_{SM} + \frac{\alpha_s}{4\pi} \frac{c_g}{\Lambda^2} (\Phi^\dagger \Phi) G_{\mu\nu}^A G^{\mu\nu A} + \left(\frac{c_t Y_t}{\Lambda^2} \bar{q}_L \tilde{\Phi}_{QR} (\Phi^\dagger \Phi) + h.c. \right). \quad (103)$$

After spontaneous symmetry breaking, the top mass is shifted,

$$m_t = \frac{Y_t v}{\sqrt{2}} \left(1 - \frac{v^2 c_t}{2\Lambda^2} \right). \quad (104)$$

The Higgs coupling to the top quark is no longer proportional to m_t and Equation (103) becomes

$$L \rightarrow \frac{\alpha_s}{4\pi} \frac{c_g}{\Lambda^2} h G_{\mu\nu}^A G^{\mu\nu A} - m_t \bar{t} t \left[1 + \frac{h}{v} \left(1 - \frac{v^2 c_t}{\Lambda^2} \right) \right] + \dots \quad (105)$$

When flavor indices are included in the fermion interactions, Equation (103) can generate flavor violation in the Higgs sector [101].

Both c_g and c_t contribute to $gg \rightarrow h$,¹⁰

$$\sigma(gg \rightarrow h) = \sigma(gg \rightarrow h)_{SM} \left(1 + 2 \frac{v^2}{\Lambda^2} (3c_g - c_t) \right) + \mathcal{O}\left(\frac{m_h^2}{m_t^2}, \frac{v^4}{\Lambda^2}\right), \quad (106)$$

and so gluon fusion cannot distinguish between c_g and c_t [102–107]. The $t\bar{t}h$ process is independent of c_g at leading order and can be used to obtain a measurement of c_t . Once radiative corrections (both QCD and electroweak) are included, however, the situation becomes murkier and the $t\bar{t}h$ rate is no longer directly proportional to c_t .

We turn now to a discussion of the effects of dimension-6 operators in the electroweak sector. As an example, we consider the SILH basis relevant for gauge-Higgs interactions [97],

$$\begin{aligned} L_{SILH} = & \frac{c_H}{2\Lambda^2} \left(\partial^\mu |\Phi|^2 \right)^2 + \frac{c_T}{2\Lambda^2} \left(\Phi^\dagger \overleftrightarrow{D}^\mu \Phi \right)^2 + \left(\frac{c_f y_f}{\Lambda^2} |\Phi|^2 \bar{f}_L \Phi f_R + h.c. \right) - \frac{c_6 \lambda}{\Lambda^2} |\phi|^6 \\ & + \frac{igc_W}{2\Lambda^2} \left(\Phi^\dagger \sigma^I \overleftrightarrow{D}^\mu \Phi \right) \left(D^\nu W_{\mu\nu}^I \right) + \frac{ig' c_B}{2\Lambda^2} \left(\Phi^\dagger \overleftrightarrow{D}^\mu \Phi \right) \left(D^\nu B_{\mu\nu} \right) \end{aligned}$$

¹⁰*Caveat emptor*: Practically every EFT paper uses different normalization and sign conventions for the EFT operators. The only way to check results like Equation (106) is to start from the definition of the operators in the Lagrangian.

$$\begin{aligned}
& + \frac{igc_{HW}}{16\pi^2\Lambda^2} \left(D^\mu \Phi \right)^\dagger \sigma^i \left(D^\nu \Phi \right) W_{\mu\nu}^i + \frac{ig'c_{HB}}{16\pi^2\Lambda^2} \left(D^\mu \Phi \right)^\dagger \left(D^\nu \Phi \right) B_{\mu\nu} \\
& + \frac{c_\gamma g'^2 g^2}{16\pi^2\Lambda^2} |\Phi|^2 B_{\mu\nu} B^{\mu\nu} + \frac{c_g g_s^2}{16\pi^2\Lambda^2} |\Phi|^2 G_{\mu\nu}^A G^{A,\mu\nu}.
\end{aligned} \tag{107}$$

Note that the normalization of the operators is arbitrary and merely reflects a prejudice about the origins of the new physics, $I = 1, 2, 3$ are $SU(2)$ indices and we have not written terms involving only fermions, or terms that do not contain a Higgs field. Many of the operators of Equation (107) introduce momentum dependence into the Higgs couplings to SM fermions and so the kinematic distributions of the Higgs will be affected.

We briefly discuss some of the phenomenological effects of Equation (107). Three of the coefficients are strongly limited by precision electroweak measurements as parameterized by the oblique parameters,

$$\begin{aligned}
\Delta T &= \frac{v^2}{\Lambda^2} c_T \\
\Delta S &= \frac{M_W^2}{\Lambda^2} (c_W + c_B).
\end{aligned} \tag{108}$$

Using the fit from Ref. [15], $|c_T| \lesssim \mathcal{O}(.03)$ and $|c_W + c_B| \lesssim \mathcal{O}(.1)$ for $\Lambda \sim 1 \text{ TeV}$.

The coefficient c_H modifies the Higgs boson kinetic energy. The physical Higgs field needs to be rescaled,

$$h \rightarrow h \left(1 - \frac{c_H v^2}{2\Lambda^2} \right), \tag{109}$$

in order to have canonically normalized kinetic energy. This shift introduces a dependence on c_H into all of the Higgs decay widths. The tree level Higgs decay widths to $\mathcal{O}(\frac{v^2}{\Lambda^2})$ in the SILH formalism are,

$$\begin{aligned}
\frac{\Gamma(h \rightarrow WW^*)}{\Gamma(h \rightarrow WW^*)|_{SM}} &= 1 - \frac{v^2}{\Lambda^2} \left[c_H - g^2 \left(c_W + \frac{c_{HW}}{16\pi^2} \right) \right] \\
\frac{\Gamma(h \rightarrow ZZ^*)}{\Gamma(h \rightarrow ZZ^*)|_{SM}} &= 1 - \frac{v^2}{\Lambda^2} \left[c_H - g^2 \left(c_W + \tan^2 \theta_W c_B + \frac{c_{HW} + \tan^2 \theta_2 c_{HB}}{16\pi^2} \right) \right] \\
\frac{\Gamma(h \rightarrow f\bar{f})}{\Gamma(h \rightarrow f\bar{f})|_{SM}} &= 1 - \frac{v^2}{\Lambda^2} (c_H + 2c_f).
\end{aligned} \tag{110}$$

The loop processes, $gg \rightarrow h$ and $h \rightarrow \gamma\gamma$, also receive corrections from the EFT operators. The expressions for Higgs decays in the SILH Lagrangian have been implemented into an update of the HDECAY program, EDECAY [108]. In the Warsaw basis, they can be obtained using the SMEFTsim code [109]. Fits to the EFT coefficients can be performed using total Higgs rates (as is done in the κ formalism) or including information from distributions [83, 110]. The kinematic information provides a significant improvement to the fits from using only the total rates.

Some of the operators of Equation (107) not only affect Higgs production, but they also change the WWZ and $WW\gamma$ vertices. Assuming CP conservation, the most general Lorentz invariant 3-gauge boson couplings can be written as [111, 112]

$$\begin{aligned}
L_V &= -ig_{WWV} \left[g_1^V (W_{\mu\nu}^+ W^{-\mu} V^\nu - W_{\mu\nu}^- W^{+\mu} V^\nu) + \kappa^V W_\mu^+ W_\nu^- V^{\mu\nu} \right. \\
&\quad \left. + \frac{\lambda^V}{M_W^2} W_{\rho\mu}^+ W^{-\mu}{}_\nu V^{\nu\rho} \right],
\end{aligned} \tag{111}$$

where $V = (Z, \gamma)$, $g_{WW\gamma} = e$, and $g_{WWZ} = g_{CW}$. In the SM, $g_1^Z = g_1^\gamma = \kappa^Z = \kappa^\gamma = 1$, $\lambda^Z = \lambda^\gamma = 0$ and $SU(2)$ gauge invariance implies,

$$\begin{aligned}\lambda^\gamma &= \lambda^Z \\ g_1^Z &= \kappa^Z + \frac{s_W^2}{c_W^2}(\kappa^\gamma - 1).\end{aligned}\tag{112}$$

The fields in Equation (111) are the canonically normalized mass eigenstate fields. These coefficients can be mapped to EFT coefficients in a straightforward manner and a subset of the dimension-6 coefficients contribute both to gauge boson pair production and Higgs production [110, 113, 114].

A consistent fit must include not only Higgs data, but also fits to anomalous gauge couplings. In Figure 21, we show fits to 3 of the EFT couplings that contribute to both W^+W^- and Higgs production, including only LEP data on W^+W^- pair production, only LHC data on W^+W^- and Higgs production, and the resulting fit combining the two. The LHC results have now surpassed the LEP results in terms of precision [110]. This figure includes the full set of dimension-6 squared contributions. In terms of the parameters of Equation (111),

$$\begin{aligned}f_W &= \frac{2\Lambda^2}{M_Z^2}(g_1^Z - 1) \\ f_B &= \frac{2\Lambda^2}{M_W^2} \left[(\kappa_\gamma - 1) - c_W^2(g_1^Z - 1) \right] \\ f_{WWW} &= \frac{4\Lambda^2}{3g^2 M_W^2} \lambda^\gamma.\end{aligned}\tag{113}$$

Global fits to EFT coefficients in the SILH basis can be found in Ref. [83, 115] and in the Warsaw basis in Ref. [113]. Many of the EFT coefficients are only weakly constrained. These results illustrate, however, that fits performed to only a single operator typically significantly overestimate the sensitivity. As of this writing, the experimental collaborations have not performed such global EFT fits.

Finally, it is interesting to ask what the target precision is for measuring EFT coefficients. In any given UV complete model, these coefficients can be calculated, and the scale Λ will be of the same order of magnitude as the mass of the new particles. This suggests that as direct searches for new particles get more and more precise, it is necessary to measure the EFT coefficients more and more precisely. In a specific UV complete model, not all coefficients will be generated, and the pattern of non-zero coefficients will be a guide to the underlying model. The EFT coefficients for numerous models with heavy scalars [116–120] and heavy vector-like quarks [121, 122] are known and suggest that measurements of $\mathcal{O}(2 - 3\%)$ will be necessary to probe models with new particles at the $2 - 3 TeV$ scale.

6 Outlook

The discovery of a SM-like Higgs boson opened a new era in particle physics. We do not yet know if we have discovered **a** Higgs boson or **the** Higgs boson. To make this determination, the measurements of Higgs interactions need to be improved to the few % level and the Higgs self-interactions need to be observed. These precision measurements will begin during the high luminosity run of the LHC, but will require a future high energy hadron collider or e^+e^- collider to reach the desired accuracy. A limiting factor will be the precision of theoretical predictions—predictions accurate at the few % level will require a dedicated effort in the coming years and improvement of our knowledge of PDFs. I have not discussed models with extra scalar particles other than the singlet model. One of the most important efforts of the Higgs program in the next few years will be the search for additional Higgs-like particles. The observation of another scalar would be the cleanest possible indication of new BSM physics in the scalar sector.

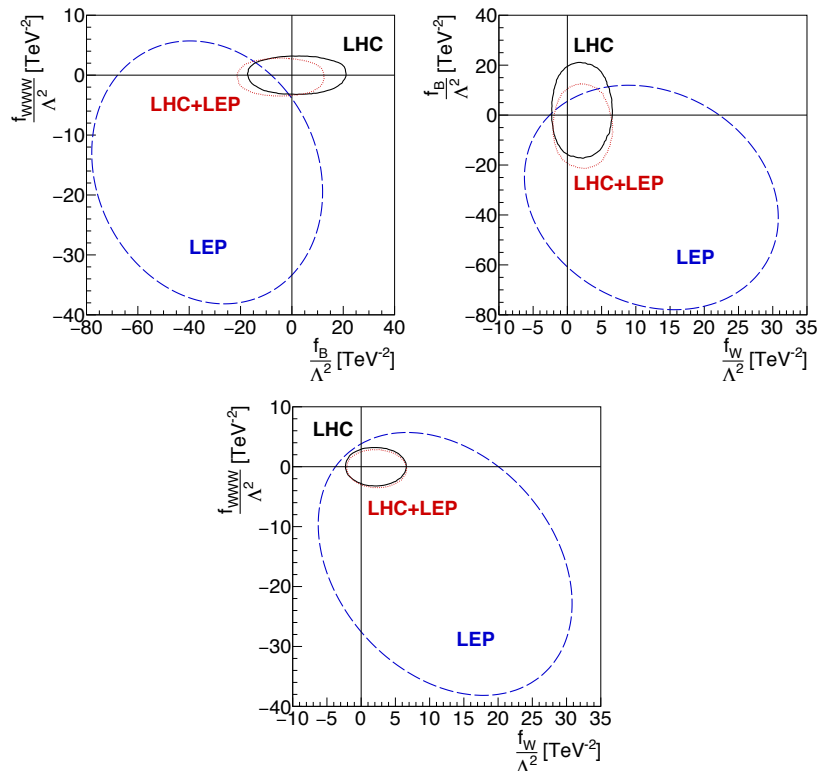


Fig. 21: Fits to LEP data, LHC data and the combination of both [110].

Acknowledgements

This work was supported by the U.S. Department of Energy under grant DE-SC0012704.

References

- [1] Georges Aad et al. Observation of a new particle in the search for the Standard Model Higgs boson with the ATLAS detector at the LHC. *Phys. Lett.*, B716:1–29, 2012.
- [2] Serguei Chatrchyan et al. Observation of a new boson at a mass of 125 GeV with the CMS experiment at the LHC. *Phys. Lett.*, B716:30–61, 2012.
- [3] S. Dawson. Introduction to electroweak symmetry breaking. In *Proceedings, Summer School in High-energy physics and cosmology: Trieste, Italy, June 29-July 17, 1998*, pages 1–83, 1998.
- [4] Abdelhak Djouadi. The Anatomy of electro-weak symmetry breaking. I: The Higgs boson in the standard model. *Phys. Rept.*, 457:1–216, 2008.
- [5] John F. Gunion, Howard E. Haber, Gordon L. Kane, and Sally Dawson. The Higgs Hunter’s Guide. *Front. Phys.*, 80:1–404, 2000.
- [6] Heather E. Logan. TASI 2013 lectures on Higgs physics within and beyond the Standard Model. 2014.
- [7] Laura Reina. TASI 2011: lectures on Higgs-Boson Physics. In *The Dark Secrets of the Terascale: Proceedings, TASI 2011, Boulder, Colorado, USA, Jun 6 - Jul 11, 2011*, pages 39–106, 2013.
- [8] Michael Spira. Higgs Boson Production and Decay at Hadron Colliders. *Prog. Part. Nucl. Phys.*, 95:98–159, 2017.
- [9] Chris Quigg. *Gauge Theories of the Strong, Weak, and Electromagnetic Interactions*. Princeton University Press, USA, 2013.

- [10] Andre de Gouvea. TASI lectures on neutrino physics. In *Physics in D \geq 4. Proceedings, Theoretical Advanced Study Institute in elementary particle physics, TASI 2004, Boulder, USA, June 6-July 2, 2004*, pages 197–258, 2004.
- [11] C. Patrignani et al. Review of Particle Physics. *Chin. Phys.*, C40(10):100001, 2016.
- [12] Georges Aad et al. Combined Measurement of the Higgs Boson Mass in pp Collisions at $\sqrt{s} = 7$ and 8 TeV with the ATLAS and CMS Experiments. *Phys. Rev. Lett.*, 114:191803, 2015.
- [13] James D. Wells. TASI lecture notes: Introduction to precision electroweak analysis. In *Physics in D \gtrsim 4. Proceedings, Theoretical Advanced Study Institute in elementary particle physics, TASI 2004, Boulder, USA, June 6-July 2, 2004*, pages 41–64, 2005.
- [14] William J. Marciano and A. Sirlin. Testing the Standard Model by Precise Determinations of W^+ and Z Masses. *Phys. Rev.*, D29:945, 1984. [Erratum: *Phys. Rev.*D31,213(1985)].
- [15] Jorge de Blas, Marco Ciuchini, Enrico Franco, Satoshi Mishima, Maurizio Pierini, Laura Reina, and Luca Silvestrini. Electroweak precision observables and Higgs-boson signal strengths in the Standard Model and beyond: present and future. *JHEP*, 12:135, 2016.
- [16] M. Baak, M. Goebel, J. Haller, A. Hoecker, D. Kennedy, R. Kogler, K. Moenig, M. Schott, and J. Stelzer. The Electroweak Fit of the Standard Model after the Discovery of a New Boson at the LHC. *Eur. Phys. J.*, C72:2205, 2012.
- [17] Michael E. Peskin and Tatsu Takeuchi. Estimation of oblique electroweak corrections. *Phys. Rev.*, D46:381–409, 1992.
- [18] Guido Altarelli and Riccardo Barbieri. Vacuum polarization effects of new physics on electroweak processes. *Phys. Lett.*, B253:161–167, 1991.
- [19] Donal O’Connell, Michael J. Ramsey-Musolf, and Mark B. Wise. Minimal Extension of the Standard Model Scalar Sector. *Phys. Rev.*, D75:037701, 2007.
- [20] Giovanni Marco Pruna and Tania Robens. Higgs singlet extension parameter space in the light of the LHC discovery. *Phys. Rev.*, D88(11):115012, 2013.
- [21] Dario Buttazzo, Giuseppe Degrassi, Pier Paolo Giardino, Gian F. Giudice, Filippo Sala, Alberto Salvio, and Alessandro Strumia. Investigating the near-criticality of the Higgs boson. *JHEP*, 12:089, 2013.
- [22] S. Dittmaier et al. Handbook of LHC Higgs Cross Sections: 1. Inclusive Observables. 2011.
- [23] A. Djouadi, J. Kalinowski, and M. Spira. HDECAY: A Program for Higgs boson decays in the standard model and its supersymmetric extension. *Comput. Phys. Commun.*, 108:56–74, 1998.
- [24] Manuel Drees and Ken-ichi Hikasa. Note on QCD corrections to hadronic Higgs decay. *Phys. Lett.*, B240:455, 1990. [Erratum: *Phys. Lett.*B262,497(1991)].
- [25] E. Braaten and J. P. Leveille. Higgs Boson Decay and the Running Mass. *Phys. Rev.*, D22:715, 1980.
- [26] Bernd A. Kniehl. Higgs phenomenology at one loop in the standard model. *Phys. Rept.*, 240:211–300, 1994.
- [27] Wai-Yee Keung and William J. Marciano. Higgs Scalar Decays: $h \rightarrow W^+W^-$. *Phys. Rev.*, D30:248, 1984.
- [28] A. Bredenstein, Ansgar Denner, S. Dittmaier, and M. M. Weber. Precision calculations for $H \rightarrow WW/ZZ \rightarrow 4\text{fermions}$ with PROPHECY4f. In *Proceedings, International Linear Collider Workshop (LCWS07 and ILC07) Hamburg, Germany, May 30-June 3, 2007, Vol.1-2*, pages 150–154, 2007.
- [29] M. Spira, A. Djouadi, D. Graudenz, and P. M. Zerwas. Higgs boson production at the LHC. *Nucl. Phys.*, B453:17–82, 1995.
- [30] D. de Florian et al. Handbook of LHC Higgs Cross Sections: 4. Deciphering the Nature of the Higgs Sector. 2016.

- [31] Charalampos Anastasiou, Claude Duhr, Falko Dulat, Elisabetta Furlan, Thomas Gehrmann, Franz Herzog, Achilleas Lazopoulos, and Bernhard Mistlberger. High precision determination of the gluon fusion Higgs boson cross-section at the LHC. *JHEP*, 05:058, 2016.
- [32] R. Keith Ellis, I. Hinchliffe, M. Soldate, and J. J. van der Bij. Higgs Decay to tau+ tau-: A Possible Signature of Intermediate Mass Higgs Bosons at the SSC. *Nucl. Phys.*, B297:221–243, 1988.
- [33] Radja Boughezal, Christfried Focke, Walter Giele, Xiaohui Liu, and Frank Petriello. Higgs boson production in association with a jet at NNLO using jetiness subtraction. *Phys. Lett.*, B748:5–8, 2015.
- [34] Radja Boughezal, Fabrizio Caola, Kirill Melnikov, Frank Petriello, and Markus Schulze. Higgs boson production in association with a jet at next-to-next-to-leading order. *Phys. Rev. Lett.*, 115(8):082003, 2015.
- [35] Falko Dulat, Bernhard Mistlberger, and Andrea Pelloni. Differential Higgs production at N^3 LO beyond threshold. 2017.
- [36] Xuan Chen, Thomas Gehrmann, Nigel Glover, and Matthieu Jaquier. Higgs plus one jet production at NNLO. *PoS*, RADCOR2015:056, 2016.
- [37] Daniel de Florian, Giancarlo Ferrera, Massimiliano Grazzini, and Damiano Tommasini. Transverse-momentum resummation: Higgs boson production at the Tevatron and the LHC. *JHEP*, 11:064, 2011.
- [38] R. P. Kauffman. Higher order corrections to Higgs boson p(T). *Phys. Rev.*, D45:1512–1517, 1992.
- [39] Pier Francesco Monni, Emanuele Re, and Paolo Torrielli. Higgs Transverse-Momentum Resummation in Direct Space. *Phys. Rev. Lett.*, 116(24):242001, 2016.
- [40] Morad Aaboud et al. Measurement of inclusive and differential cross sections in the $H \rightarrow ZZ^* \rightarrow 4\ell$ decay channel in pp collisions at $\sqrt{s} = 13$ TeV with the ATLAS detector. *JHEP*, 10:132, 2017.
- [41] Albert M Sirunyan et al. Measurements of properties of the Higgs boson decaying into the four-lepton final state in pp collisions at $\sqrt{s} = 13$ TeV. *JHEP*, 11:047, 2017.
- [42] Fabrizio Caola and Kirill Melnikov. Constraining the Higgs boson width with ZZ production at the LHC. *Phys. Rev.*, D88:054024, 2013.
- [43] Nikolas Kauer. Interference effects for $H \rightarrow WW/ZZ \rightarrow \ell\bar{\nu}_\ell\bar{\ell}\nu_\ell$ searches in gluon fusion at the LHC. *JHEP*, 12:082, 2013.
- [44] Vardan Khachatryan et al. Constraints on the Higgs boson width from off-shell production and decay to Z-boson pairs. *Phys. Lett.*, B736:64–85, 2014.
- [45] Georges Aad et al. Constraints on the off-shell Higgs boson signal strength in the high-mass ZZ and WW final states with the ATLAS detector. *Eur. Phys. J.*, C75(7):335, 2015.
- [46] Aleksandr Azatov, Christophe Grojean, Ayan Paul, and Ennio Salvioni. Taming the off-shell Higgs boson. *Zh. Eksp. Teor. Fiz.*, 147:410–425, 2015. [*J. Exp. Theor. Phys.*120,354(2015)].
- [47] James S. Gainer, Joseph Lykken, Konstantin T. Matchev, Stephen Mrenna, and Myeonghun Park. Beyond Geolocating: Constraining Higher Dimensional Operators in $H \rightarrow 4\ell$ with Off-Shell Production and More. *Phys. Rev.*, D91(3):035011, 2015.
- [48] Christoph Englert, Yotam Soreq, and Michael Spannowsky. Off-Shell Higgs Coupling Measurements in BSM scenarios. *JHEP*, 05:145, 2015.
- [49] John M. Campbell, R. Keith Ellis, and Ciaran Williams. Bounding the Higgs width at the LHC using full analytic results for $gg \rightarrow e^-e^+\mu^-\mu^+$. *JHEP*, 04:060, 2014.
- [50] Sally Dawson et al. Working Group Report: Higgs Boson. In *Proceedings, 2013 Community Summer Study on the Future of U.S. Particle Physics: Snowmass on the Mississippi (CSS2013): Minneapolis, MN, USA, July 29-August 6, 2013*, 2013.
- [51] V. Del Duca, W. Kilgore, C. Oleari, C. Schmidt, and D. Zeppenfeld. Gluon fusion contributions to $H + 2$ jet production. *Nucl. Phys.*, B616:367–399, 2001.

- [52] A. Stange, William J. Marciano, and S. Willenbrock. Associated production of Higgs and weak bosons, with $h \rightarrow b\bar{b}$, at hadron colliders. *Phys. Rev.*, D50:4491–4498, 1994.
- [53] Oliver Brein, Robert V. Harlander, and Tom J. E. Zirke. $vh@nnlo$ - Higgs Strahlung at hadron colliders. *Comput. Phys. Commun.*, 184:998–1003, 2013.
- [54] Ansgar Denner, Stefan Dittmaier, Stefan Kallweit, and Alexander Muck. Electroweak corrections to Higgs-strahlung off W/Z bosons at the Tevatron and the LHC with HAWK. *JHEP*, 03:075, 2012.
- [55] Albert M Sirunyan et al. Inclusive search for a highly boosted Higgs boson decaying to a bottom quark-antiquark pair. 2017.
- [56] Morad Aaboud et al. Evidence for the $H \rightarrow b\bar{b}$ decay with the ATLAS detector. 2017.
- [57] Jonathan M. Butterworth, Adam R. Davison, Mathieu Rubin, and Gavin P. Salam. Jet substructure as a new Higgs search channel at the LHC. *Phys. Rev. Lett.*, 100:242001, 2008.
- [58] Matthew D. Schwartz. TASI Lectures on Collider Physics. 2017.
- [59] S. Dawson, C. Jackson, L. H. Orr, L. Reina, and D. Wackerroth. Associated Higgs production with top quarks at the large hadron collider: NLO QCD corrections. *Phys. Rev.*, D68:034022, 2003.
- [60] S. Dawson, L. H. Orr, L. Reina, and D. Wackerroth. Associated top quark Higgs boson production at the LHC. *Phys. Rev.*, D67:071503, 2003.
- [61] W. Beenakker, S. Dittmaier, M. Kramer, B. Plumper, M. Spira, and P. M. Zerwas. NLO QCD corrections to t anti-t H production in hadron collisions. *Nucl. Phys.*, B653:151–203, 2003.
- [62] W. Beenakker, S. Dittmaier, M. Kramer, B. Plumper, M. Spira, and P. M. Zerwas. Higgs radiation off top quarks at the Tevatron and the LHC. *Phys. Rev. Lett.*, 87:201805, 2001.
- [63] S. Frixione, V. Hirschi, D. Pagani, H. S. Shao, and M. Zaro. Weak corrections to Higgs hadroproduction in association with a top-quark pair. *JHEP*, 09:065, 2014.
- [64] S. Frixione, V. Hirschi, D. Pagani, H. S. Shao, and M. Zaro. Electroweak and QCD corrections to top-pair hadroproduction in association with heavy bosons. *JHEP*, 06:184, 2015.
- [65] S. Dawson, S. Dittmaier, and M. Spira. Neutral Higgs boson pair production at hadron colliders: QCD corrections. *Phys. Rev.*, D58:115012, 1998.
- [66] Daniel de Florian and Javier Mazzitelli. Higgs pair production at next-to-next-to-leading logarithmic accuracy at the LHC. *JHEP*, 09:053, 2015.
- [67] Daniel de Florian, Massimiliano Grazzini, Catalin Hanga, Stefan Kallweit, Jonas M. Lindert, Philipp Maierhöfer, Javier Mazzitelli, and Dirk Rathlev. Differential Higgs Boson Pair Production at Next-to-Next-to-Leading Order in QCD. *JHEP*, 09:151, 2016.
- [68] Daniel de Florian, Ignacio Fabre, and Javier Mazzitelli. Higgs boson pair production at NNLO in QCD including dimension 6 operators. 2017.
- [69] Daniel de Florian and Javier Mazzitelli. Higgs Boson Pair Production at Next-to-Next-to-Leading Order in QCD. *Phys. Rev. Lett.*, 111:201801, 2013.
- [70] Jonathan Grigo, Kirill Melnikov, and Matthias Steinhauser. Virtual corrections to Higgs boson pair production in the large top quark mass limit. *Nucl. Phys.*, B888:17–29, 2014.
- [71] S. Borowka, N. Greiner, G. Heinrich, S. P. Jones, M. Kerner, J. Schlenk, and T. Zirke. Full top quark mass dependence in Higgs boson pair production at NLO. *JHEP*, 10:107, 2016.
- [72] G. Heinrich, S. P. Jones, M. Kerner, G. Luisoni, and E. Vryonidou. NLO predictions for Higgs boson pair production with full top quark mass dependence matched to parton showers. *JHEP*, 08:088, 2017.
- [73] R. Frederix, S. Frixione, V. Hirschi, F. Maltoni, O. Mattelaer, P. Torrielli, E. Vryonidou, and M. Zaro. Higgs pair production at the LHC with NLO and parton-shower effects. *Phys. Lett.*, B732:142–149, 2014.
- [74] Search for pair production of Higgs bosons in the $b\bar{b}b\bar{b}$ final state using proton–proton collisions at $\sqrt{s} = 13$ TeV with the ATLAS detector. Technical Report ATLAS-CONF-2016-049, CERN,

- Geneva, Aug 2016.
- [75] Search for Higgs boson pair production in the final state containing two photons and two bottom quarks in proton-proton collisions at $\sqrt{s} = 13$ TeV. Technical Report CMS-PAS-HIG-17-008, CERN, Geneva, 2017.
 - [76] Higgs Pair Production in the $H(\rightarrow \tau\tau)$ and $H(\rightarrow b\bar{b})$ channel at the High-Luminosity LHC. Technical Report ATL-PHYS-PUB-2015-046, CERN, Geneva, Nov 2015.
 - [77] Chien-Yi Chen, S. Dawson, and I. M. Lewis. Exploring resonant di-Higgs boson production in the Higgs singlet model. *Phys. Rev.*, D91(3):035015, 2015.
 - [78] Alan J. Barr, Matthew J. Dolan, Christoph Englert, Danilo Enoque Ferreira de Lima, and Michael Spannowsky. Higgs Self-Coupling Measurements at a 100 TeV Hadron Collider. *JHEP*, 02:016, 2015.
 - [79] Raul Costa, Margarete Mühlleitner, Marco O. P. Sampaio, and Rui Santos. Singlet Extensions of the Standard Model at LHC Run 2: Benchmarks and Comparison with the NMSSM. *JHEP*, 06:034, 2016.
 - [80] S. Dawson and M. Sullivan. Enhanced di-Higgs Production in the Complex Higgs Singlet Model. 2017.
 - [81] S. Dawson and I. M. Lewis. NLO corrections to double Higgs boson production in the Higgs singlet model. *Phys. Rev.*, D92(9):094023, 2015.
 - [82] Giuseppe Degrassi, Pier Paolo Giardino, Fabio Maltoni, and Davide Pagani. Probing the Higgs self coupling via single Higgs production at the LHC. *JHEP*, 12:080, 2016.
 - [83] Stefano Di Vita, Christophe Grojean, Giuliano Panico, Marc Riembau, and Thibaud Vantalon. A global view on the Higgs self-coupling. *JHEP*, 09:069, 2017.
 - [84] Graham D. Kribs, Andreas Maier, Heidi Rzehak, Michael Spannowsky, and Philip Waite. Electroweak oblique parameters as a probe of the trilinear Higgs boson self-interaction. *Phys. Rev.*, D95(9):093004, 2017.
 - [85] Wojciech Bizon, Martin Gorbahn, Ulrich Haisch, and Giulia Zanderighi. Constraints on the trilinear Higgs coupling from vector boson fusion and associated Higgs production at the LHC. *JHEP*, 07:083, 2017.
 - [86] Georges Aad et al. Measurements of the Higgs boson production and decay rates and constraints on its couplings from a combined ATLAS and CMS analysis of the LHC pp collision data at $\sqrt{s} = 7$ and 8 TeV. *JHEP*, 08:045, 2016.
 - [87] Measurement of the Higgs boson coupling properties in the $H \rightarrow ZZ^* \rightarrow 4\ell$ decay channel at $\sqrt{s} = 13$ TeV with the ATLAS detector. Technical Report ATLAS-CONF-2017-043, CERN, Geneva, Jul 2017.
 - [88] Measurements of Higgs boson properties in the diphoton decay channel with 36.1 fb^{-1} pp collision data at the center-of-mass energy of 13 TeV with the ATLAS detector. Technical Report ATLAS-CONF-2017-045, CERN, Geneva, Jul 2017.
 - [89] Evidence for the decay of the Higgs Boson to Bottom Quarks. Technical Report CMS-PAS-HIG-16-044, CERN, Geneva, 2017.
 - [90] Higgs to WW measurements with 15.2 fb^{-1} of 13 TeV proton-proton collisions. Technical Report CMS-PAS-HIG-16-021, CERN, Geneva, 2017.
 - [91] Measurements of properties of the Higgs boson decaying into four leptons in pp collisions at $\sqrt{s} = 13$ TeV. Technical Report CMS-PAS-HIG-16-041, CERN, Geneva, 2017.
 - [92] Georges Aad et al. Measurements of the Higgs boson production and decay rates and coupling strengths using pp collision data at $\sqrt{s} = 7$ and 8 TeV in the ATLAS experiment. *Eur. Phys. J.*, C76(1):6, 2016.
 - [93] Vardan Khachatryan et al. Precise determination of the mass of the Higgs boson and tests of

- compatibility of its couplings with the standard model predictions using proton collisions at 7 and 8 TeV. *Eur. Phys. J.*, C75(5):212, 2015.
- [94] Ilaria Brivio and Michael Trott. The Standard Model as an Effective Field Theory. 2017.
- [95] W. Buchmuller and D. Wyler. Effective Lagrangian Analysis of New Interactions and Flavor Conservation. *Nucl. Phys.*, B268:621–653, 1986.
- [96] Kaoru Hagiwara, S. Ishihara, R. Szalapski, and D. Zeppenfeld. Low-energy effects of new interactions in the electroweak boson sector. *Phys. Rev.*, D48:2182–2203, 1993.
- [97] G. F. Giudice, C. Grojean, A. Pomarol, and R. Rattazzi. The Strongly-Interacting Light Higgs. *JHEP*, 06:045, 2007.
- [98] Adam Falkowski, Benjamin Fuks, Kentarou Mawatari, Ken Mimasu, Francesco Riva, and Veronica sanz. Rosetta: an operator basis translator for Standard Model effective field theory. *Eur. Phys. J.*, C75(12):583, 2015.
- [99] James D. Wells and Zhengkang Zhang. Effective theories of universal theories. *JHEP*, 01:123, 2016.
- [100] Roberto Contino, Adam Falkowski, Florian Goertz, Christophe Grojean, and Francesco Riva. On the Validity of the Effective Field Theory Approach to SM Precision Tests. *JHEP*, 07:144, 2016.
- [101] Roni Harnik, Joachim Kopp, and Jure Zupan. Flavor Violating Higgs Decays. *JHEP*, 03:026, 2013.
- [102] Aleksandr Azatov, Christophe Grojean, Ayan Paul, and Ennio Salvioni. Resolving gluon fusion loops at current and future hadron colliders. *JHEP*, 09:123, 2016.
- [103] Roberto Contino, Margherita Ghezzi, Christophe Grojean, Margarete Muhlleitner, and Michael Spira. Effective Lagrangian for a light Higgs-like scalar. *JHEP*, 07:035, 2013.
- [104] Chien-Yi Chen, S. Dawson, and I. M. Lewis. Top Partners and Higgs Boson Production. *Phys. Rev.*, D90(3):035016, 2014.
- [105] Florian Goertz, Andreas Papaefstathiou, Li Lin Yang, and JosÁl Zurita. Higgs boson pair production in the D=6 extension of the SM. *JHEP*, 04:167, 2015.
- [106] Aleksandr Azatov, Roberto Contino, Giuliano Panico, and Minhõ Son. Effective field theory analysis of double Higgs boson production via gluon fusion. *Phys. Rev.*, D92(3):035001, 2015.
- [107] M. Gillioz, R. Grober, C. Grojean, M. Muhlleitner, and E. Salvioni. Higgs Low-Energy Theorem (and its corrections) in Composite Models. *JHEP*, 10:004, 2012.
- [108] Roberto Contino, Margherita Ghezzi, Christophe Grojean, Margarete Mühlleitner, and Michael Spira. eHDECAY: an Implementation of the Higgs Effective Lagrangian into HDECAY. *Comput. Phys. Commun.*, 185:3412–3423, 2014.
- [109] Ilaria Brivio, Yun Jiang, and Michael Trott. The SMEFTsim package, theory and tools. 2017.
- [110] Anja Butter, Oscar J. P. Eboli, J. Gonzalez-Fraile, M. C. Gonzalez-Garcia, Tilman Plehn, and Michael Rauch. The Gauge-Higgs Legacy of the LHC Run I. *JHEP*, 07:152, 2016.
- [111] K. J. F. Gaemers and G. J. Gounaris. Polarization Amplitudes for $e^+e^- \rightarrow W^+W^-$ and $e^+e^- \rightarrow ZZ$. *Z. Phys.*, C1:259, 1979.
- [112] Kaoru Hagiwara, R. D. Peccei, D. Zeppenfeld, and K. Hikasa. Probing the Weak Boson Sector in $e^+e^- \rightarrow W^+W^-$. *Nucl. Phys.*, B282:253–307, 1987.
- [113] Laure Berthier, Mikkel Bjorn, and Michael Trott. Incorporating doubly resonant W^\pm data in a global fit of SMEFT parameters to lift flat directions.
- [114] Adam Falkowski, Martin Gonzalez-Alonso, Admir Greljo, David Marzocca, and Minhõ Son. Anomalous Triple Gauge Couplings in the Effective Field Theory Approach at the LHC. *JHEP*, 02:115, 2017.
- [115] Adam Falkowski and Francesco Riva. Model-independent precision constraints on dimension-6 operators. *JHEP*, 02:039, 2015.

- JHEP*, 09:157, 2016.
- [116] Sally Dawson and Christopher W. Murphy. Standard Model EFT and Extended Scalar Sectors. *Phys. Rev.*, D96(1):015041, 2017.
- [117] J. de Blas, J. C. Criado, M. Perez-Victoria, and J. Santiago. Effective description of general extensions of the Standard Model: the complete tree-level dictionary. 2017.
- [118] Brian Henning, Xiaochuan Lu, and Hitoshi Murayama. How to use the Standard Model effective field theory. *JHEP*, 01:023, 2016.
- [119] Johann Brehmer, Ayres Freitas, David Lopez-Val, and Tilman Plehn. Pushing Higgs Effective Theory to its Limits. *Phys. Rev.*, D93(7):075014, 2016.
- [120] Martin Gorbahn, Jose Miguel No, and Veronica Sanz. Benchmarks for Higgs Effective Theory: Extended Higgs Sectors. *JHEP*, 10:036, 2015.
- [121] Chien-Yi Chen, S. Dawson, and Elisabetta Furlan. Vectorlike fermions and Higgs effective field theory revisited. *Phys. Rev.*, D96(1):015006, 2017.
- [122] J. A. Aguilar-Saavedra. A Minimal set of top-Higgs anomalous couplings. *Nucl. Phys.*, B821:215–227, 2009.